Strength characterization of wood to wood connections using stress field analysis

By

Mitchell G. Shope

B.S. Mechanical Engineering
University of Tennessee Knoxville, College of Engineering (2015)

SUBMITTED TO THE DEPARTMENT OF CIVIL AND ENVIRONMENTAL ENGINEERING IN PARTIAL FULFILLMENT OF THE REQUIREMENTS OF THE DEGREE OF

MASTER OF ENGINEERING IN CIVIL AND ENVIRONMENTAL ENGINEERING
AT THE
MASSACHUSETTS INSTITUTE OF TECHNOLOGY

JUNE 2016

Signature of Author: Signature redacted
Department of Civil and Environmental Engineering
May 10th, 2016

Certified by: Signature redacted
Cyrentin Fivet
Lecturer of Civil and Environmental Engineering
Thesis Co-Supervisor

Certified by: Signature redacted
John Ochsendorf
Class of 1942 Professor of Civil and Environmental Engineering and Architecture
Thesis Co-Supervisor

Accepted by: Signature redacted
Heidi M. Nepf
Donald and Martha Harleman Professor of Civil and Environmental Engineering
Chair, Departmental Committee for Graduate Program

Strength characterization of wood to wood connections using stress field analysis

by

Mitchell Shope

Submitted to the Department of Civil and Environmental Engineering on May 9th, 2016
In Partial Fulfillment of the Requirements for the Degree of
Master of Engineering in Civil and Environmental Engineering

ABSTRACT

Minimizing construction cost and material usage are two dominant aspects in structural design. As a building material, timber presents a cheap, renewable option. However, current practice favors steel connections for wood structures. Wood to wood connections offer a solution to the minimization of steel connections. While some wood-only connections are referenced in timber codes, small modifications to these designs as well as a multitude of other possible connection types are yet to be characterized. This thesis analyzes wood to wood joints with stress fields. Stress field analyses may quickly and easily enable the design of timber joints and characterize the maximum loads they can handle.

First, this thesis surveys and interconnects the theoretical concepts of wood behavior, plastic design, stress fields, and graphic statics. Additionally, this thesis tests these relationships empirically by load testing a designed double-birdsmouth connection and observing inconsistencies between the theoretical stress field model, code-required strength, and physical tests. The thesis shows that stress fields are a suitable design approach when considering the design of this wood-wood joint. The results also show that careful consideration must be attributed to the material properties of the wood as well as the possible failure modes. This thesis finally shows that shear failure should be checked in addition to compressive and tensile failure and provides a quick method to ensure a safe design.

Thesis Co-Supervisor: John Ochsendorf
Title: Professor of Civil and Environmental Engineering and Architecture

Thesis Co-Supervisor: Corentin Fivet
Title: Lecturer of Civil and Environmental Engineering

Acknowledgements

This thesis is dedicated to my wonderful and loving mother, Robin Shope, for which none of this year could have ever happened. Thank you for teaching me a tireless work ethic and to continue to push myself further and achieve more than I thought possible, even when I continue to resist.

I additionally want to thank my father Frank Shope for his incessant words of advice and encouragement as well as his ability to truly live by example. Although I may have resisted working for long periods of the day, I can finally say with 70 pages of proof that you have instilled in me a desire to exceed expectations and work until the job is finished.

More thanks to my lovely girlfriend Marlee Houk for her willingness to put up with long talks of engineering nonsense and wood theory. Thanks for always pushing me to remember how blessed I am to be provided with all of the opportunities I have had this year.

Thank you to my brother Connor Shope for offering the support and ability to unplug for a couple hours a week in deep strategic planning to keep my mind sharp and tactful.

An unquantifiable abundance of thanks to Corentin Fivet for the absurd amount of hours discussing wood theory, graphic statics, plastic theory, and generally discussing what the hell was happening inside a piece of wood. I am forever grateful for your dedication to teaching and to your students, and you've made this a fantastic year at MIT for the entire MEng program.

Thanks to John Ochsendorf for the continual support and encouragement to join the MIT community. Your zeal and fervor for structural engineering as well as the little chocolate cream cakes at the open house are what really drew me in to attending MIT.

More thanks to Chris Dewart for his immense help in the ordering, handling, and fabrication of the wood used in the tests.

Thank you to Stephen Rudolph for his abundance of help in making the testing of the joints possible. This thesis would not have happened without his consul and support.

I would also really like to extend a special thank you to Ron Anthony for his advice and expertise in the physical domain of wood design. Without his experience and background, the results and contributions of this thesis would remain largely unclear.

Last word of thanks to all of my MEng cohort, this year wouldn't have been possible without all of the support and collaboration from each of you. I will forever remember all of the blood, sweat, and flaming wax that we shared together in the MEng room.

Table of Contents

List of Figures

List of Tables

Chapter 1 - Introduction

Section 1.1 - Background

Although considered one of the world's oldest building materials, wood has recently taken a secondary role to other structural materials like concrete and steel. Despite its low cost and renewability, timber has been chiefly neglected due to its lower effective tensile strength and lack of homogeneity compared to steel. However, because of recent developments in wood technology like cross-laminated timbers (CLT) that augment the allowable stress in wood design, timber is returning as a more universally viable structural material.

While timber may never have as intrinsically high allowable stresses as steel, it offers numerous benefits and advantages over its metal counterpart. In the current market, wood is significantly cheaper than steel. Moreover, wood can be easier to assemble and more fire resistant because of the way that wooden beams char (Ritter 1990). Perhaps most importantly, wood as a structural material is renewable and a carbon sink; according to the United States Energy Information Administration, buildings account for nearly half of the energy consumption in the United States (2016). When considering the amount of CO_2 emissions that are invested into framing a structure, steel generates several tons of carbon while structural wood continues to absorb carbon similarly to its life cycle. As a result, wooden buildings could potentially have a beneficial net emissions compared to carbon-consuming steel, concrete, or glass structures.

Section 1.2 – Research Motivation

Minimizing construction cost and steel dependency, then, becomes even more important in wooden building design. While steel can be used as a reinforcing material and connector for wooden beams and trusses, designs that eliminate or reduce steel reinforcement and connections are truly ideal. Wood-only connections offer a possible solution to the reduction of steel connections, however the strength classification and determination of these connections is widely unknown. In fact, in the American Wood Council National Design Specifications for Wood Construction, there are no wood to wood connection details or specifications and only a half-page on the compressive bearing strength of angled wooden beams (2015).

Furthermore, in existing literature and codes on wood connection design, there are very strict dimensioning requirements and preset ratios that must be followed for most connections. As such, there is little to no

ability to modify existing joints and no capability of designing new joints. With such limited information on the actual strength capacities of existing joints, designing wood to wood connections becomes nothing more than a cut-and-paste routine with minimal input from the designer. A method of characterizing the strength capacity of a wide variety of wood to wood connections quickly and accurately therefore becomes very valuable in theory and in practice.

This thesis seeks to test the applicability of stress field models to predict the failure loads and modes of wooden members and connections. As stated previously, having an accurate and simple method of characterizing the flow of forces throughout wooden beams is imperative to understanding how to best design these members. While stress fields have been used widely in concrete design through the formation of strut and tie models, the orthotropic nature of wood has prevented its simplified modeling and analysis with discontinuous stress fields. Furthermore, because it is not ductile in tension, wood has limited tensile plastic design and exhibits brittle failure at its tensile limits.

Wood is a unique substance in that its allowable strength not only differs in tension and compression but is also heavily dependent on the angle of the grain inside the wood. As such, the classical strut-and-tie model usually used in concrete becomes much more complex as the stresses change severely according to the angle of incident force. The stresses, therefore, do not flow through wooden beams as intuitively expected but tend to follow the grain of the wood much more closely. Indeed, the compressive and tensile strengths parallel to the grain of the wood are typically on the order of ten to twenty times their perpendicular counterpart. While this makes the "correct" stress fields more difficult to predict, the formation of these theoretical models is almost identical to that of concrete, requiring little further knowledge or intuition to create. As such, most practicing engineers familiar with concrete design could apply the same fundamentals, making this method relatively easy to learn and therefore widely applicable.

Section 1.3 – Problem Statement

While stress field theory seems applicable to wood strength and wooden connections, its accuracy compared to empirical testing has never been fully analyzed. Therefore, in order to obtain an approximate assessment of the validity of stress field modeling of wooden connections, physical models must be constructed and tested. The results from the physical testing will be compared both to the stress field models created as well as the code-prescribed strength approximations to create a hierarchy of connection strength values.

The tested connection is termed a "double birdsmouth joint" and can be seen in Figure 1-1. The geometry of this joint is built according to a research study by Julius Natterer in 2000; the geometric and construction detailing can be found in Chapter 3. While the scope of this thesis is limited to the investigation of this singular joint, the theory of stress fields and their applicability to wooden connection design can be extrapolated to many other circumstances as well.

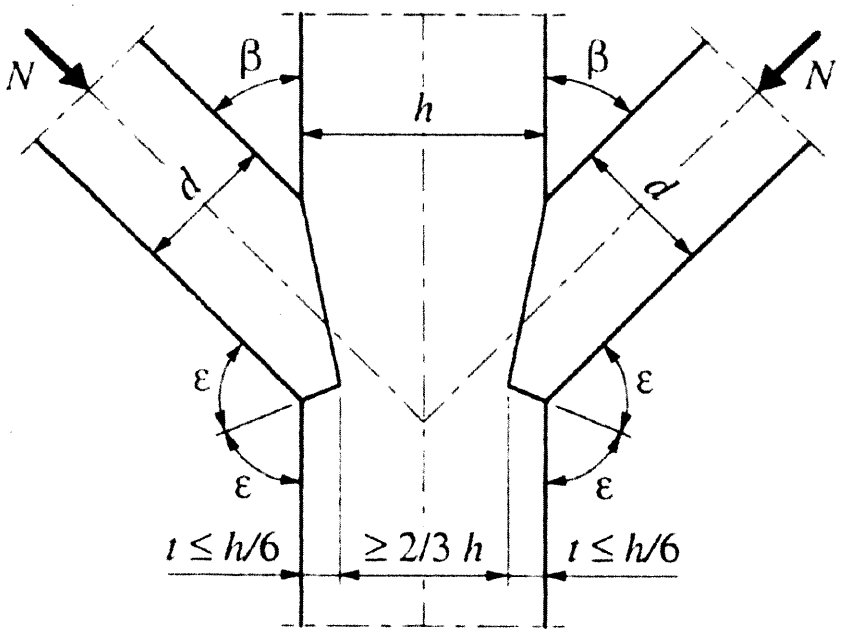

Figure 1-1. Double birdsmouth joint (Natterer 2000)

Section 1.4 – Research Objectives

From these tests, this paper seeks to identify the relationship between stress field analysis and empirical testing. These values will also be compared back to the code-prescribed standards to identify the relationship between all three sets of data. Furthermore, these tests aim to show the controlling failure mode of the chosen connection detail and decipher if this mode can be similarly modeled through stress field analysis. Finally, any critical modes of failure and discrepancies between code-generated connection strength and empirical testing will be identified and analyzed.

Chapter 2 – Literature Review

This chapter serves to supplement the findings in this study by presenting an understanding of wood mechanics, wooden connection design, plastic theory, and stress field theory in both concrete and wood design. The chapter is broken up accordingly into the five topics mentioned above.

Section 2.1 – Wood Science and Mechanics

Although wood is an extremely common and well-known construction material, its properties and characteristics differ from any other type of building resource. While a full knowledge of wood anatomy is not essential to understand the structural performance of this living building material, a working, fundamental awareness of the common characteristics that affect the strength and performance of wood in structural design is very valuable.

While there are dozens of species of wood in use throughout the United States, lumber is split into two general groups: hardwoods and softwoods. Although the name is counterintuitive, the classification of a species as a hardwood or softwood is not based on its relative hardness; indeed, many softwood species are actually harder than most low- to medium-density hardwoods (Ritter 1990). The nomenclature difference between species actually refers to its biological makeup of its reproductive structure. Hardwood trees are *angiosperms*, which produce seeds with a sort of covering, while softwoods are *gymnosperms* which allow seeds to spread uncovered (Kollman 1968). Whereas hardwoods are commonly used in carpentry, flooring, and small-scale applications, softwoods dominate the structural usage of wood (Ritter 1990).

A simple model of the wood microstructure depicts a group of wood cells as a bundle of drinking straws as seen in Figure 2-1. Compared to their relative weight, the straws are capable of resisting a considerable load in compression parallel to their longitudinal axis (when neglecting lateral buckling). However, when loaded perpendicularly to this axis, the straws yield under a much smaller load. While a simplistic analysis, this model helps to demonstrate why the compressive strength of wood varies so drastically dependent on the orientation of the grain angle (or longitudinal axis). For most species of softwood, the compressive strength of wood parallel to the grain is on the order of nine to ten times the strength perpendicular to the grain (Ritter 1990). As such, designs that favor loading parallel to the orientation of the wood grain are ideal.

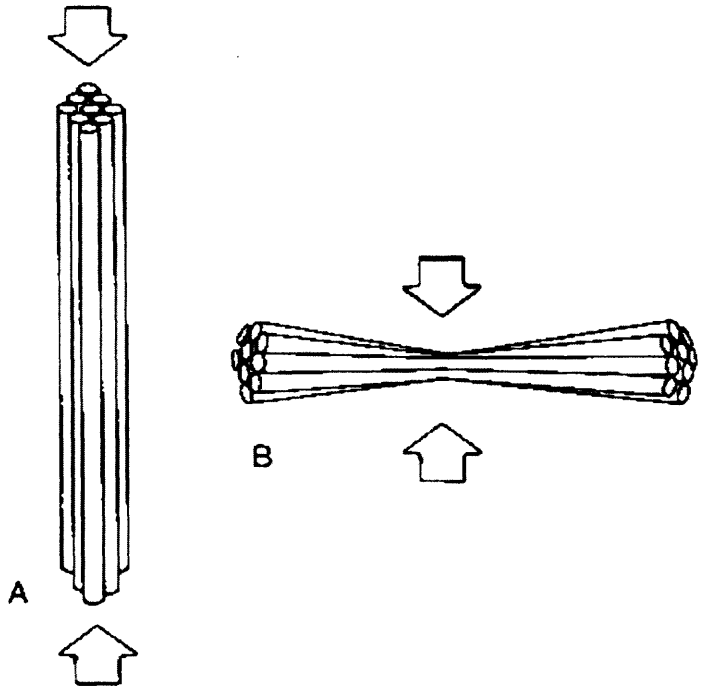

Figure 2-1. Portrayal of wooden cell structure when loaded in compression (A) parallel to their longitudinal axis and (B) perpendicular to their longitudinal axis (Ritter 1990)

The same analogy can be used to demonstrate the incredibly poor performance of wood loaded in tension perpendicular to the grain. In this drinking straw model, it is easy to see that there is essentially *no* tension strength perpendicular to the grain; in reality there is a small tension strength, although most building codes advise against this form of loading at all as it is unpredictable and is greatly influenced by defects within the wood (AWC NDS 2015). Wood in tension parallel to the grain, nonetheless, is the strongest axis of possible loading for a wooden specimen.

Perhaps the most identifiable but least-known aspect of wood characterization is its grain pattern and orthotropy. Isotropic materials like steel, glass, and other metals have properties that are independent of angle or orientation; in other words, they behave the same in tension and compression regardless of location or direction in the material. On the other hand, anisotropic materials possess characteristics that vary across two axes. Most composites are anisotropic as they have different transverse strength than they do longitudinal. Although wood is anisotropic, it can be further identified as orthotropic, a sub-classification of anisotropy, in which the material strength is dependent on three mutually perpendicular axes: the longitudinal direction, the radial direction, and the tangential direction (Ritter 1990). These axes can be seen more closely in Figure 2-2.

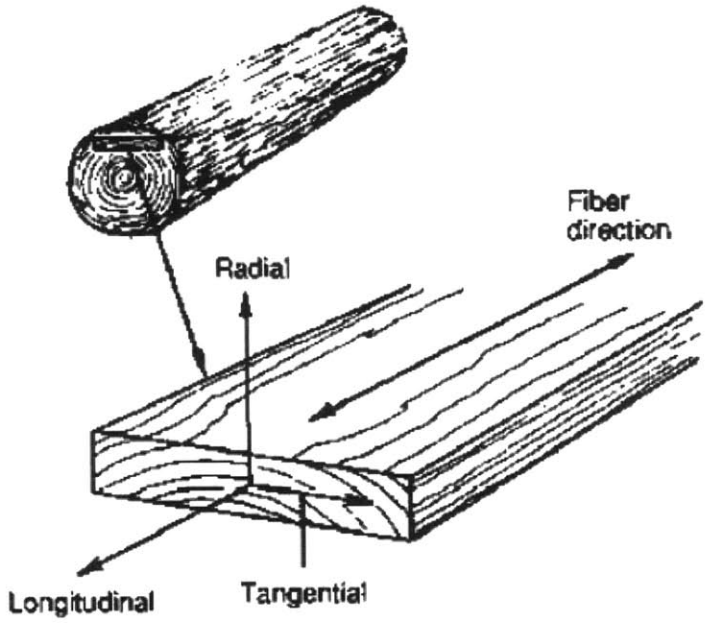

Figure 2-2. Principal axes of wood and grain orientation. (Ritter 1990)

In isotropic materials like steel, the mechanical properties are related by three elastic constants; the modulus of elasticity (E), shear modulus (G), and Poisson's ratio (μ). In an orthotropic material like wood, on the other hand, twelve constants are required to describe the elastic range; three moduli of elasticity, three shear moduli, and six Poisson's ratios (Ritter 1990). Furthermore, these constants vary among species and are heavily dependent on other factors like moisture content and specific gravity. However, while wood does follow this orthotropic model in small-scale timbers, the differences between the radial and tangential axes are usually very small compared to the differences in the longitudinal orientation in practice, and they are completely randomized when a tree is cut into lumber. As a result, wood strength values are usually generalized and given for just directions parallel to the grain (which follows the longitudinal axis) and perpendicular to the grain (which follows the tangential axis) (Ritter 1990).

When loaded in compression, as discussed previously, wood behaves very differently depending on longitudinal grain orientation. When parallel with the grain, each wood cell behaves similarly to a hollow column that bends and receives lateral support from the multitude of adjacent cells around it. As such, at failure, large deformations govern as the internal crushing of the wood is reached. Conversely, when loaded perpendicular to the grain, the wood cells collapse onto one another at a much lower load. Recalling the straw example demonstrated above, the straws sink together until all of the hollow cavities are collapsed.

As a result, the compressive strength of wood perpendicular to the grain becomes strong after these voids are filled; there is no longer a hollow space between the tubes. Failure, then, is governed by a loss in utility and deformation rather than fracture or crushing (Ritter 1990). An industry-standard value of a 0.04 inch deformation is allowable, which increases the nominal strength of compression perpendicular to the grain at no deformation. The increase in this allowable limit is between 1.5 to 2 times the original allowable stress (ASTM 2555 2015).

Wood loaded in tension also typically follows the grain, but with some key differences. Conversely to compression, wood in tension parallel to the grain shows little to no deformation before brittle fracture. Similarly, tension perpendicular to the grain is characterized by limited deformation and brittle fracture. Wood performs very well in tension when loaded parallel to the grain, roughly twice as strong as in compression, however when loaded perpendicular to the grain, the tensile strength drops drastically to as little as one twentieth of its parallel counterpart (ASTM 2555 2015). As such, almost all codes and specifications urge the avoidance of designs that incorporate tension perpendicular to the grain (AWC NDS 2015).

However, while designs that favor tension and compression directly in line with the grain pattern of the timber are ideal, there are occasions where the wood must be loaded in a perpendicular fashion or at an angle to the grain. When wood is loaded in compression at an angle to the grain as in Figure 2-3, a combination of compression forces both parallel and perpendicular to the grain are present within the member.

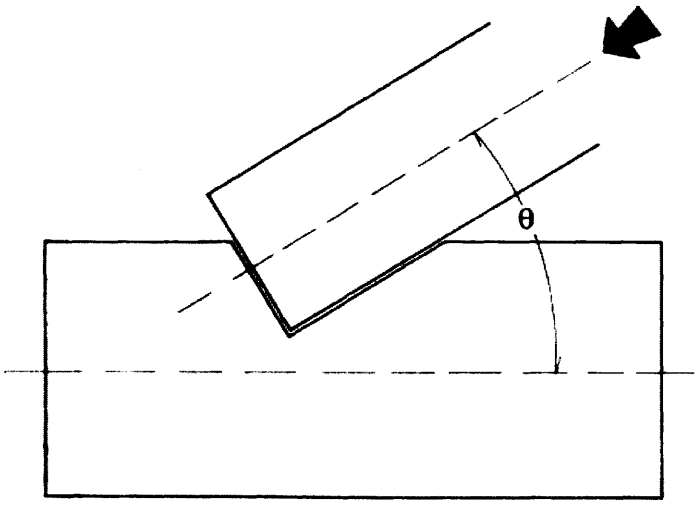

Figure 2-3. Wood loaded in compression at an angle to the grain (AWC NDS 2015)

An empirical formula was determined by Hankinson in 1921 that predicted very accurately the compression strength of a member loaded at an angle to the grain. While this formula was originally found for loads in spruce members, it actually shows remarkable accuracy for almost every species of wood and has been adopted to be universally applicable for wood (Hankinson 1921). Hankinson's formula can also be used when considering both tension and shear at an angle to the grain. Hankinson's formula can be seen in Equation 2-1, where σ is the allowable stress of the wood at angle alpha, parallel to the grain, or perpendicular to the grain, depending on subscript.

$$\sigma_\alpha = \frac{\sigma_\parallel * \sigma_\perp}{\sigma_\parallel * \sin^n \alpha + \sigma_\perp * \cos^n \alpha} \quad (Eq. 2-1)$$

The values of n are acceptable between 1.5 and 2, however are most frequently just taken to be 2. This formula provides an accurate prediction of the allowable stress in a wooden member loaded at an angle and is used extensively throughout this study as well as in practice. A diagram showing the wood strength at varying angles in tension (left half of circle) and compression (right half of circle) according to the Hankinson formula is shown in Figure 2-4 (Fivet 2012). The values are listed for different specifications of wood in the European codes.

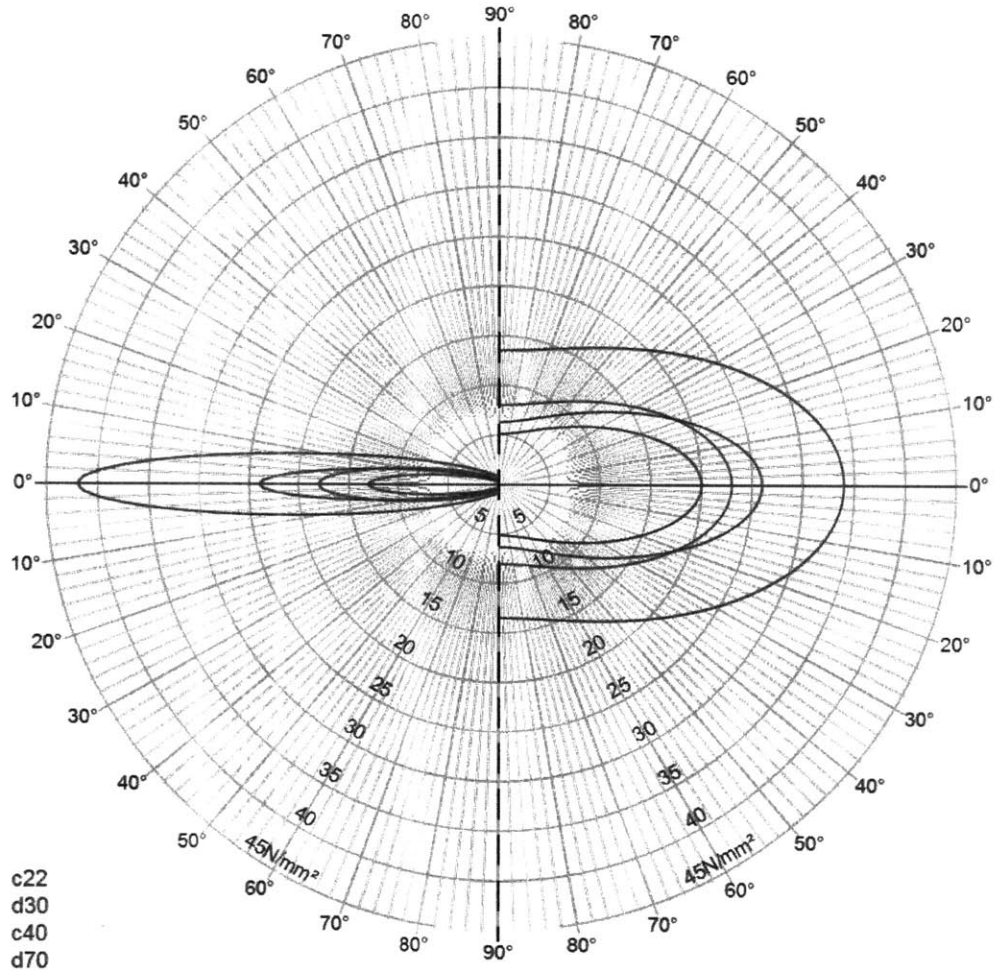

Figure 2-4. Allowable strength in compression (right) and tension (left) at varying angles for various wood qualities (Fivet 2012)

Finally, there are several intrinsic characteristics in wood design that can affect the nominal strength of the wood. Properties such as moisture content, specific gravity, knots, and grain slope all affect the strength of wood, however their effects are hard to quantify and generalize for specific design (Ritter 1990). Because of these flaws and defects that are typically randomized, lumber is visually inspected and graded, whether by a man or machine, into different groups and classifications. Boards free of knots or imperfections are obviously a better and stronger material, but are also much more expensive and difficult to find.

When considering the tensile strength of a wooden member, each section of the wood must be fully considered. The most frequent failure criteria is almost always located around an imperfection or flaw within the wood. Moreover, as the size of board increases or dimensions increase, there is a significantly higher likelihood of an imperfection, thus a greater chance of tensile failure. This phenomena is referred to

as Weibull's weakest-link theory, which accounts for the lowering of fracture stress in members as their size is increased (Weibull 1961). Because full-scale testing of each project is not possible, small clear wood specimens must be tested and their strength values extrapolated. So, while a laboratory test may show a small, clear wood specimen to have a very high tensile strength, these values are reduced drastically as members are scaled up and imperfections are present in the materials. This weakest-link theory is important to consider when comparing the discrepancies between small-scale testing and full-scale code-prescribed precedents.

In American practice, lumber is typically rough-sawn to predetermined shapes and sizes which vary down from one inch thickness up to eight or ten inch thickness. After the lumber has been rough-cut, it is then milled down to have nice, smooth edges. This reduces the board width typically by one-half inch. As a result, there is a discrepancy between the nominal and physical dimensions of a board. For instance, a two-by-four board refers to a board that was rough cut to be two inches thick and four inches wide. A two-by-four in usage, though, is actually a 3.5"x1.5" board (Engineering Toolbox 2016). This dimensional difference is essential to remember when considering board dimensions and fabricating actual joints.

Section 2.2 – Wood-only Connection Design

Although there are hundreds of wood-wood connections and designs, very few are actually specified and characterized for actual loads. The bulk of wood-wood connections are found in small-scale carpentry and architecture where loading is not as much of a consideration compared to aesthetics and fit. However, for structural joints of timber-framed buildings, they can be split into two main categories; compression connections, such as the birdsmouth, and tension connections, such as mortise-tenon joints with pegs. This study focuses on the application of compression connections but is expandable to other types of connections as well. Two compression connections are portrayed in Figure 2-5 as examples of possible connection types.

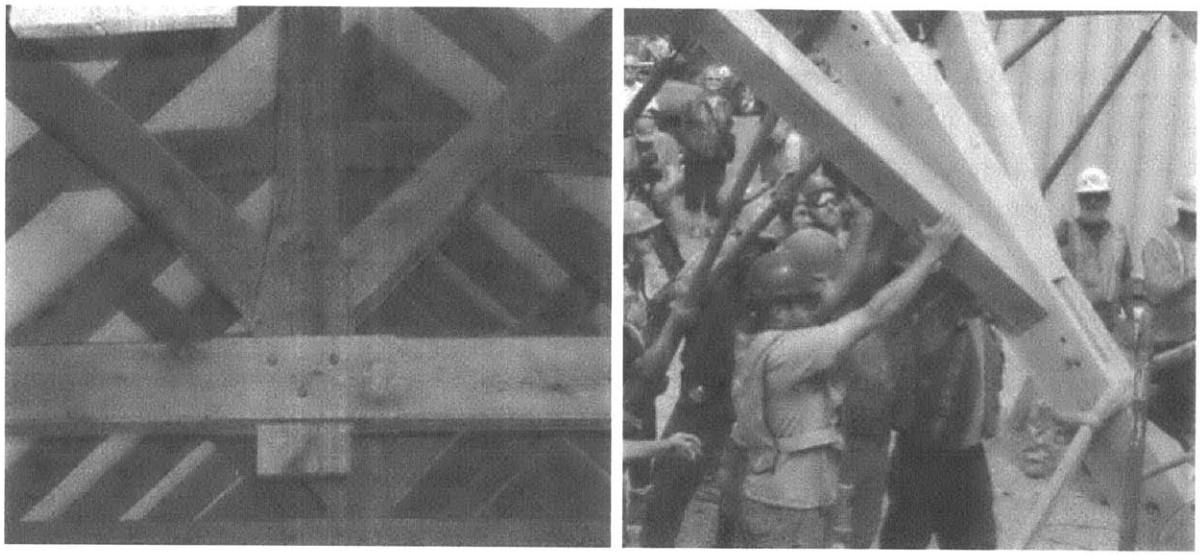

Figure 2-5. Sample timber-framed compression connections (Timber Framers Guild 2016)

In the American Wood Council (AWC) design codes, there is no information, characterization, or mention of wood to wood connections in the general guidelines or the supplemental information (AWC NDS 2015). Classic metal-less connections are neglected, and indeed the only piece of information pertaining to wooden joints is a half-page explanation of the Hankinson formula and the bearing strength of wood at an angle to the grain. In order to find any sort of strength or design criteria for these types of joints, an extensive search must be conducted through research papers or organizational documents like those found in the Timber Framer's Guild or the Timber Frame Engineering Council. Even in these highly specialized and specific establishments, pure wood connection details are rare and complex with very little ability for modification.

One such connection that has been studied and characterized is the standard birdsmouth connection shown in Figure 2-6. This connection is very common in a roof truss where the roof members are bearing a compressive load down onto the tension beams below. This connection along with two others was studied and characterized by Natterer (2000) to offer some designability of birdsmouth joints, however these research papers are neither in building codes nor even in English, so their applicability to American timber design is not fully realized.

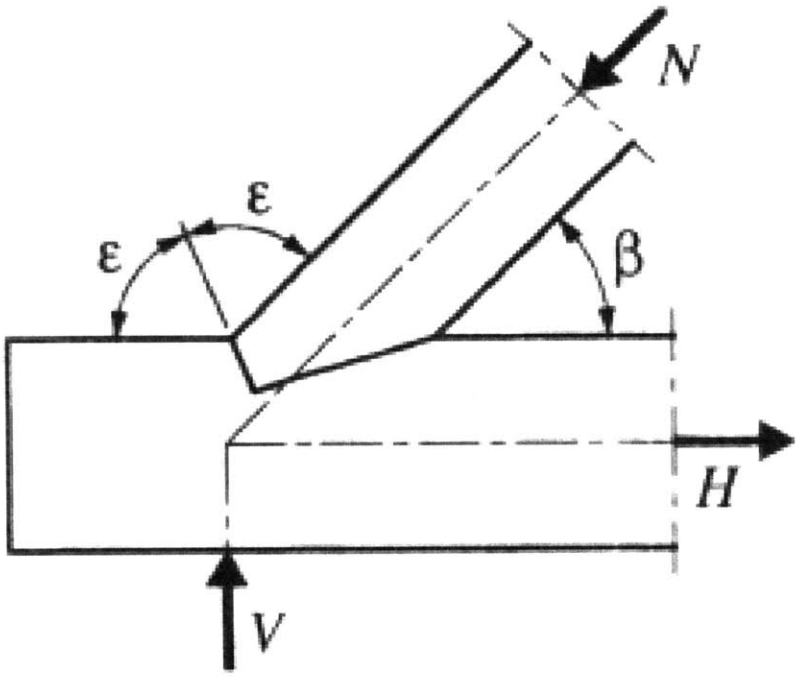

Figure 2-6. Standard birdsmouth connection
(Natterer 2000)

Section 2.3 – Plastic Theory

To fully understand how the theory of plasticity may apply to wood design, a fundamental awareness of plastic theory in its current practice and form must be implicit. In elastic theory, which dominates most of the current design coding and practice, materials are allowed to be loaded up to their yield stress. Because steel is one of the most common and widely used building materials, it will be used as a baseline explanation.

As seen in Figure 2-7, the yield strength of a material is located at the point where the Young's Modulus stops being a straight line. At this point, the strain increases with little or no increase in loading, meaning there is deformation in the sample. The elastic theory of design only allows loads up to this yield strength where all deformations are recovered when the loading is removed. However, there is a region after the yield strength; called the plastic region; where the material (in this case steel) can take loads even above the yield strength as it continues to deform. This region is called "plastic" because the deformation exerted on the sample cannot be removed after the loading stops; in other words, the deformation becomes

permanent compared to its elastic counterpart. In the case of Grade 60 steel, the difference between the yield strength and ultimate strength is 60 kips to 96 kips, respectively (Engineering Toolbox 2016).

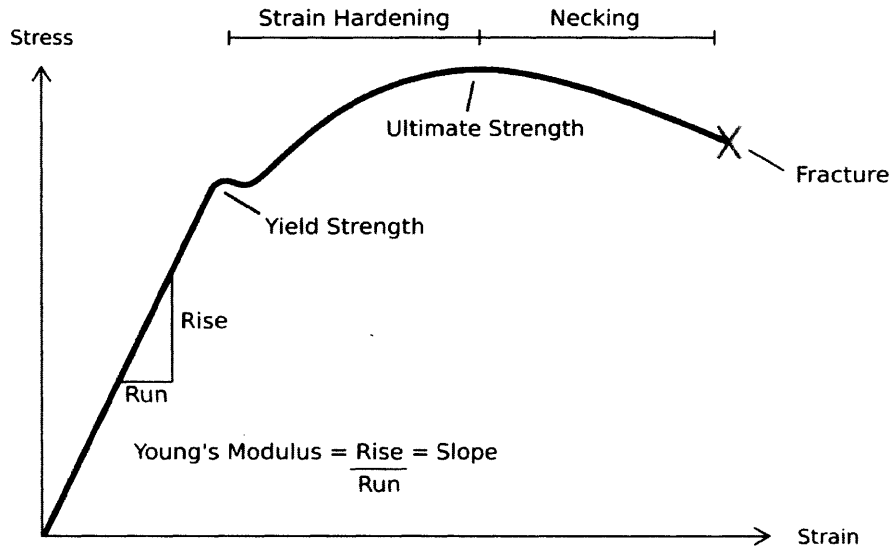

Figure 2-7. Stress-strain curve for steel (Breakey 2008)

Plastic theory, then, yields very different results compared to elasticity. Typically, elastic theory controls deformations and serviceability checks while plastic theory can allow for larger loads for a given material (Muttoni 1997). When determining the collapse load of a system, three conditions must be satisfied at collapse. First, the structure must be in equilibrium; that is, the internal bending moments must be in equilibrium with the external loads. The internal bending moments, then, must everywhere be less than or at most equal to the plastic moment capacity of the material. Finally, there must be an arrangement of plastic hinges that will allow for deformation of the structure with no additionally induced load. These conditions are named the equilibrium condition, yield condition, and mechanism condition, respectively (Muttoni 1997).

The first two requirements can be lumped into one circumstance in which the structure must be statically admissible, or under a loading case where both equilibrium and yield are satisfied (Muttoni 1997). A system load P_1 can be induced that ensures that both yield and equilibrium conditions are met, and for each system there is exists a largest values P_1^{max}. The mechanism condition is satisfied by having a kinematically admissible system, or a load that produces full deformation of plastic zones without additional load (Gvozdev 1938; 1960). This condition can be characterized by a load P_2, and when all deformations in the

structure are considered, a minimum load P_2^{min} can be identified. At collapse, then, all three conditions are satisfied as seen in Equations 2-2 and 2-3.

$$P_1^{max} \leq P_{collapse} \leq P_2^{min} \; (Eq. 2-2)$$

$$P_1^{max} = P_2^{min} \; (Eq. 2-3)$$

From these conditions, three fundamental theorems of plastic design can be extrapolated. Firstly, the lower bound theorem states that any value P_1 which satisfies an equilibrium state and the yield condition is a lower bound on the values of the real collapse load: $P_1 \leq P_{collapse}$. In other words, any design load P_1 that is found to function in equilibrium for a given system is an acceptable load for the structure. Secondly, the upper bound theorem is the converse and says that any value P_2 which is calculated from an arrangement of plastic hinges creates an upper bound on the collapse load, or $P_{collapse} \leq P_2$. Finally, the collapse load $P_{collapse}$ has a definite and unique solution, $P_{collapse} = P_1^{max} = P_2^{min}$. This theorem is named the uniqueness theorem. These three rules govern plastic design and its implementation in practice (Muttoni 1997). A comparison of the conditions versus the theorem solutions can be seen in Table 2-1.

Table 2-1. Summary of plastic theory (adapted from Muttoni 1997)

Condition	Static Solution	Complete Solution	Kinematic Solution
Equilibrium Condition	Satisfied	Satisfied	Satisfied
Yield Condition	Satisfied	Satisfied	Not Satisfied
Mechanism Condition	Not Satisfied	Satisfied	Satisfied
Result	Lower Bound $P_1 \leq P_{collapse}$	Collapse Load $P_{collapse}$	Upper Bound $P_2 \geq P_{collapse}$
Method	Static Method	--	Mechanism Method

Timber, however, works slightly differently than steel as a plastic material. While steel follows a very similar stress-strain curve in both tension and compression, the stress-strain curves for wood are very different and are characterized by extremely dissimilar fracture results (Brunner 2000). As seen referring back to Figure 2-7, steel undergoes a high amount of elongation before fracture, sometimes ranging up to roughly 250% strain. When loaded in compression, wood does exhibit a similar ductile behavior to steel, however the fracture range for wood is much lower with a strain in the 10-15% strain region (Brunner 2000). Furthermore, wood loaded in tension has an almost non-existent plasticity; there is almost no observable ductility as wood in tension undergoes brittle fracture at its failure state. Figure 2-8 shows the

stress-strain curve for wood loaded parallel to the grain compared to the curves of both steel and concrete for comparison.

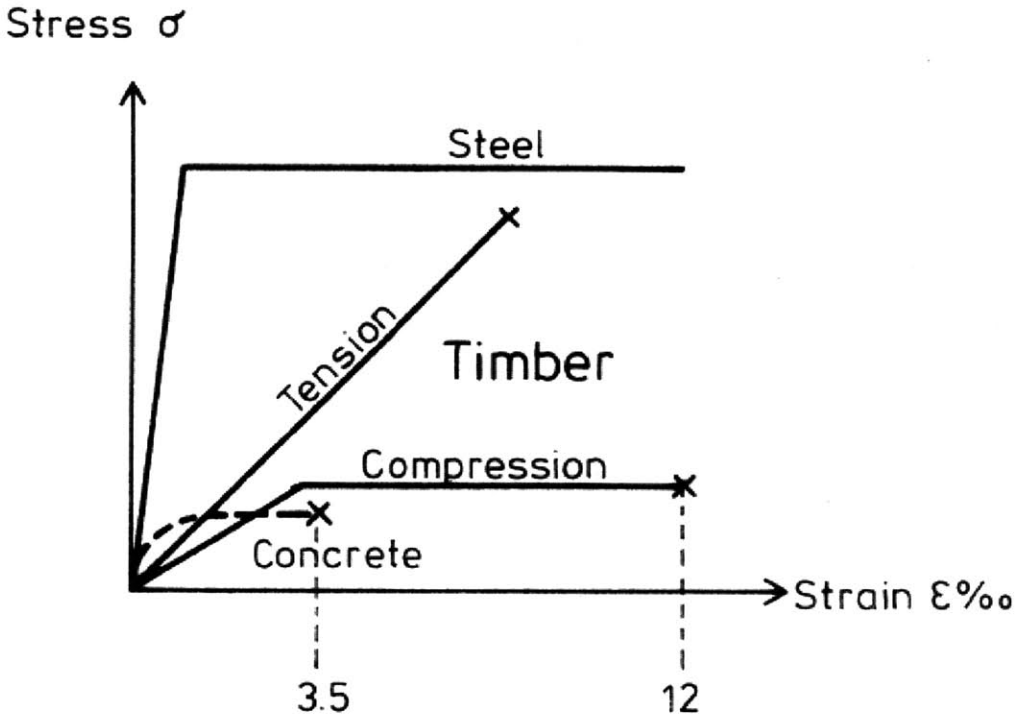

Figure 2-8. Stress-strain curve for timber among other materials (wood loaded parallel to grain) (Brunner 2000)

Section 2.4 – Stress Fields in Concrete Design

While stress fields and strut-and-tie models are often interchanged synonymously, they each have very different origins and meanings. Today, however, both are used primarily for the design and reinforcement detailing of structural concrete. The strut-and-tie model is loosely based on the truss analogy, a method that was developed on intuition to describe after the fact why and where reinforced concrete was cracking (Ruiz 2007). Conversely, stress fields were developed directly in line with the theory of plasticity and applied to concrete as well as steel and masonry. Drucker continued later by Jacques Heyman and others initiated plastic stress field design in the early sixties which paved the way to modern stress field analysis (Drucker 1960; Muttoni 1997; Heyman 2008).

At the onset of elastic stress field design, Schlaich et al. (1987) proposed a method for developing truss models named the "strut-and-tie model". For a given element and load, a resulting truss that resists such a load becomes a model of the forces throughout the member. Schlaich et al. continues to explain that in

cases with various possible truss models, the resulting truss with the minimum strain energy for the entire system is the most suitable truss model (1987). This principle is referred to as the minimum energy principle, in which loads will travel through a structure in the path that minimizes the strain energy to the material. This theorem is similar to path of least resistance proposal in electrical circuits; in a circuit, current will flow through the path that offers the least resistance.

Since the nineteen-eighties, though, truss models and stress fields have been generically combined systematically for the analysis of structural concrete. Because of the multitude of possible discontinuous stress fields, also referred to as strut-and-tie action, that can result from a structural member and given load, the development of stress fields is chiefly based on intuition and previous experience.

As the strut-and-tie model has been used more widely throughout practice, its fundamentals of design have become more straight-forward and simplified. While all structural components are three-dimensional, most stress field models utilize two-dimensional projections to simplify the understanding of the force flow throughout the structure.

In order to broadly understand the application of stress fields and the strut-and-tie model, a brief overview of the formation of these models is presented in this thesis. Pictured in Figure 2-9 is a sample reinforced concrete deep beam with a given load F and reaction R. In order to resolve this force down to the reaction, a compression strut must be drawn between F and R. To rectify the angled force from the strut, a tension tie is needed near the reaction force R and a horizontal compression strut is needed at the top near the incident force F (Kostic 2009).

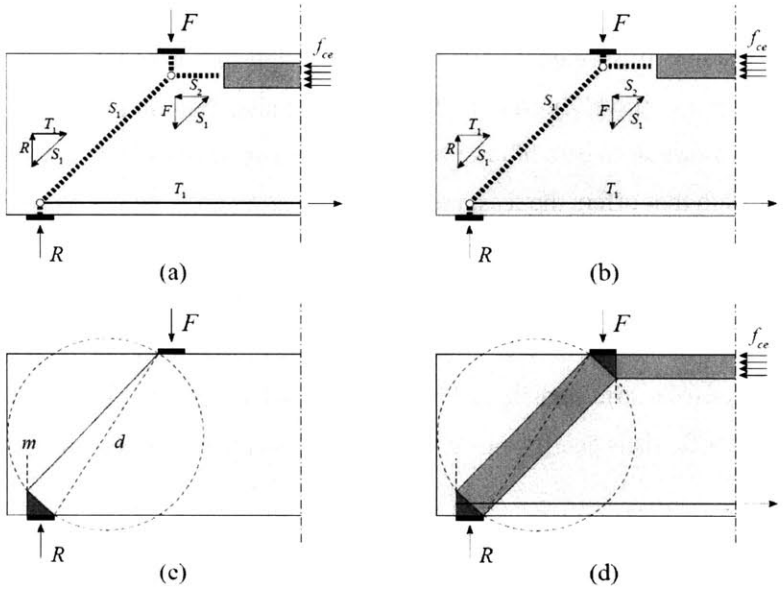

Figure 2-9. Strut-and-tie model of simplified deep beam example and corresponding discontinuous stress field (Kostic 2009)

Even if the magnitude of the incident force F is not known, the relative magnitude between F, S_1, and S_2 can be found by drawing a force triangle at the top node. As shown in Figure 2-9 (a), an arbitrary thickness is chosen for S_2 which keeps the stress field, indicated by the dark grey rectangle, within the geometry of the beam at all times. As this thickness is increased, the resulting thicknesses of F and S_1 also change as their magnitude is dependent on that of S_2. From this stage, it is an iterative process to identify which zone is "controlling"; i.e. which compression zone has the largest possible stress before its stress field exceeds the possible size of the given geometry. After dictating the controlling stress zone, all other stress fields can be scaled according to the stress in the controlling zone based on their respective forces. Because tension is taken by steel reinforcing within the concrete, the tension zone remains as a solid line while the finalized compression zones show discrete fields as seen in Figure 2-9 (d) (Kostic 2009).

It is also possible to design geometry from a given stress field. If the incident force F is known, then the value of F would dictate the stress field thickness of every other field. From these criteria, a simple process of sizing a beam around the given stress field would result. Keep in mind, however, that these stress fields are discrete, discontinuous approximations of stress within the member whereas the real result is always a continuous flow of forces throughout the entire geometry. However, this simple example serves to demonstrate how a set of forces can be resolved throughout a concrete member to identify necessary regions and sizing of steel reinforcement (Kostic 2009).

Figure 2-10 shows another example of a strut-and-tie model through a reinforced concrete deep beam. In this example, there are several discrete point loads, F, which must be taken down to a reaction R. As a continuance from the previous example, the total vertical force is split into four equal forces. Similarly to the above example, this model is constructed piece-by-piece. In (a), the reaction force as well as the tensile force in the reinforcement member are known (assumed to be identical from the previous example). From this assumption and knowing the magnitude of the force F, a resultant strut can be calculated (seen in (b)). A continual process finds the resulting struts and finally the horizontal compression strut pictured in (d).

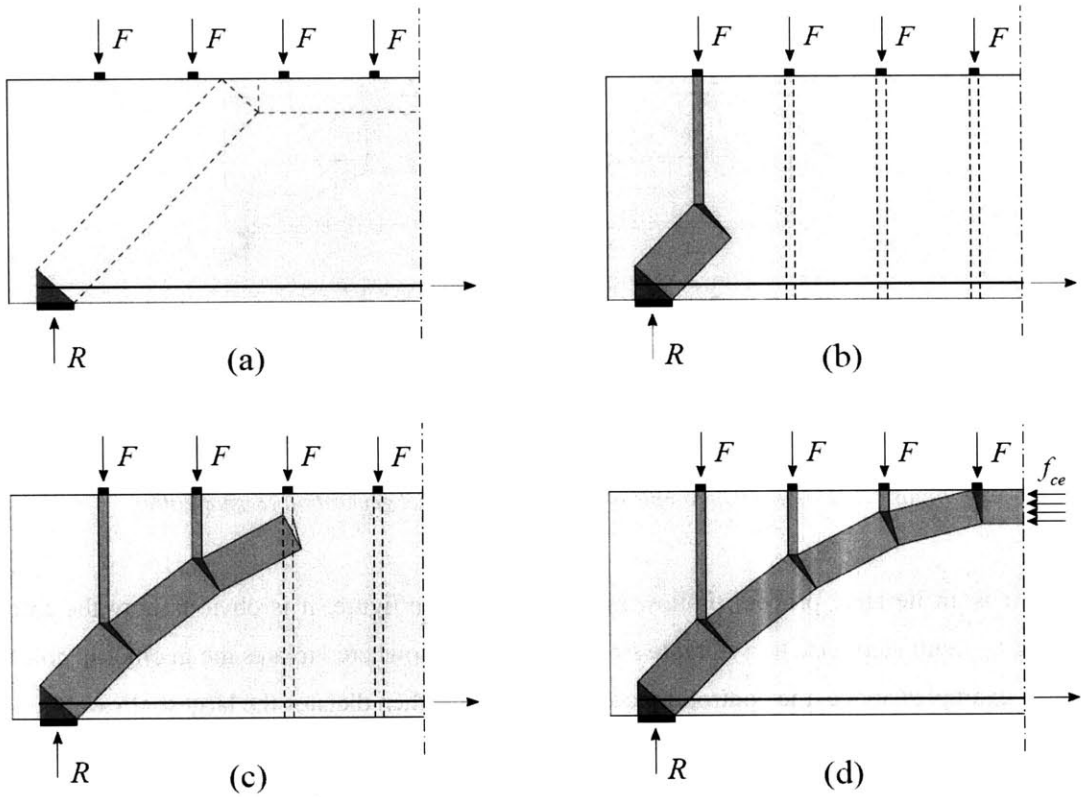

Figure 2-10. Discrete stress field for multiple concentrated loads (Kostic 2009)

A final example demonstrating the iterative nature of strut-and-tie model construction is shown in Figure 2-11. In (a), the simplest truss model possible is constructed. Obviously, this truss violates the physical constraints of the geometry presented. However, by getting a baseline starting point, a simple modification can then be made in (b); splitting the truss with a compression strut that is then tied horizontally to the right reaction. In practice, having either vertical or horizontal reinforcement is standard, so specifying a strut-and-tie model with all tension forces resulted vertically or horizontally is ideal.

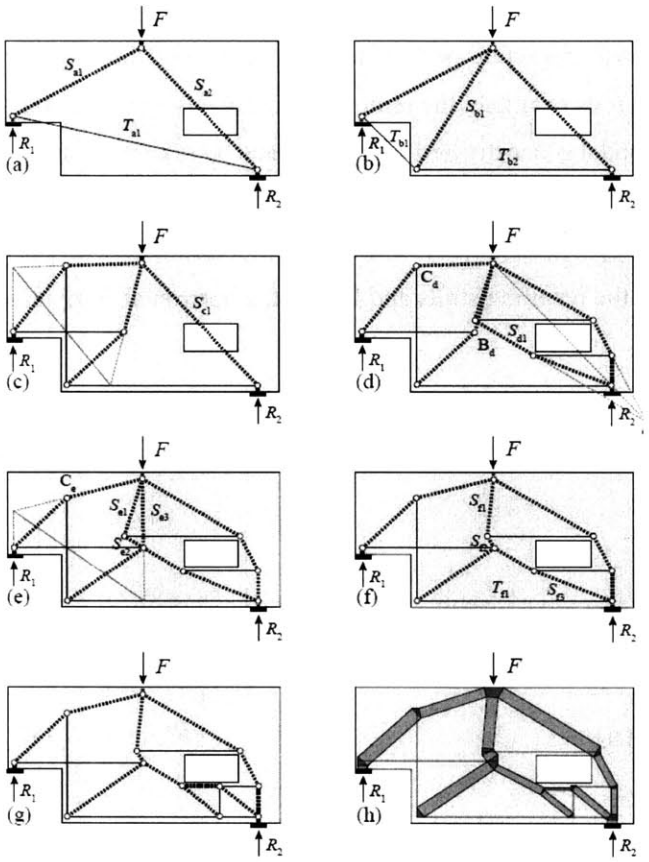

Figure 2-11. Iterative example of strut-and-tie model generation (Kostic 2009)

From here it is an iterative process. Following the steps in the figure, it is obvious how the forces are transformed to result step-wise to a suitable stress field which nowhere violates the geometric constraints. As with the examples above, the controlling compression zone then dictates the largest allowable stress in the system, and the incident force *F* can be quantified from this zone (as shown in (h)).

Careful consideration must be given to the nodal regions when constructing strut-and-tie models (Muttoni 1997). As seen in Figure 2-12, there are four possible node configurations for three intersecting forces to be in equilibrium: all compression, all tension, two compression-one tension, or two tension-one compression. When these three forces come together at this nodal point, they must be in static equilibrium with each other. If the incident forces are not in equilibrium, the resulting system is therefore not in equilibrium, and one of the force orientations must be changed (Muttoni 1997).

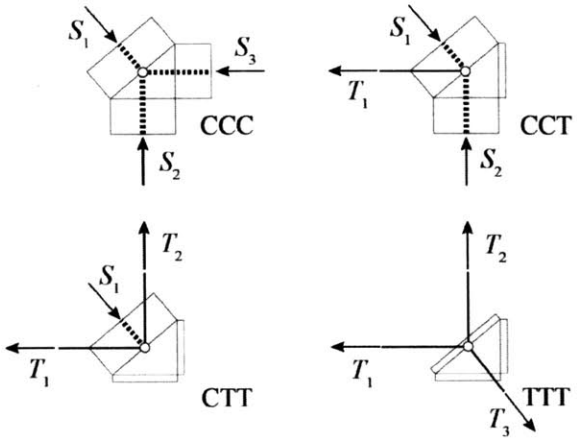

Figure 2-12. Possible nodal configurations for intersecting forces (Kostic 2009)

The nodal regions themselves contain a stress field as shown in Figure 2-13. In this biaxial stress state, both principal stresses are equal to the allowable stress of the material. For three forces coming in at angles not orthogonal to each other, the forces must be shown to be in equilibrium with each other or the nodal region will not be stable. The stress within the nodes is generally not checked; empirically, if the rectangular stress field leading into the node is allowable by the material, then the stress within the node will be suitable (Marti 1985).

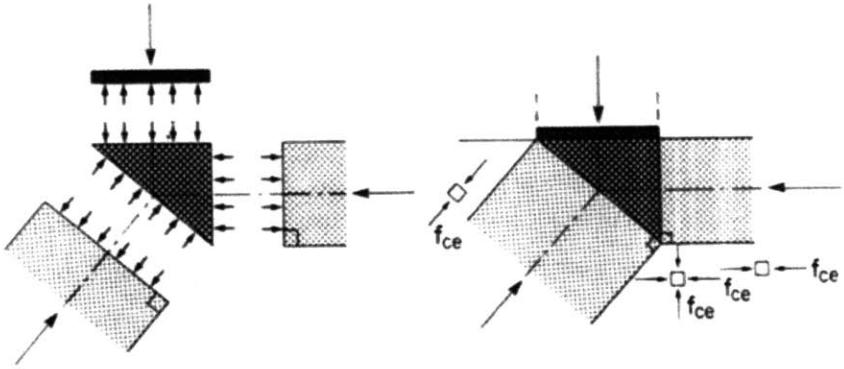

Figure 2-13. Biaxial stress in nodal region (Muttoni 1997)

Because a closed force triangle can be drawn to determine equilibrium at each nodal point, a full force diagram outlining the entire strut-and-tie network can be constructed to demonstrate the static equilibrium of the entire structure. Graphic statics; or graphically demonstrating the orientation and magnitude of forces throughout the structure with vector addition and positioning; is an incredibly useful tool when designing

these strut-and-tie networks (Allen et al 2010). Graphic statics not only provides all forces throughout the structure but also guarantees equilibrium. Furthermore, with the combination of a force diagram and a form diagram, the strain energy of the system is easily calculable, and a comparison between models can therefore be quickly and simply made.

Section 2.5 – Graphic Statics

Graphic statics is grounded in a relationship between two diagrams: the force diagram, which is representative of the forces in members, and the form diagram, which is the actual physical form of the structure. The form diagram is measured in units of length whereas the length of members in the force diagram represent the magnitude of forces in those members (Allen et al 2010). A form diagram is seen in Figure 2-14 (a) and its corresponding force diagram in (b).

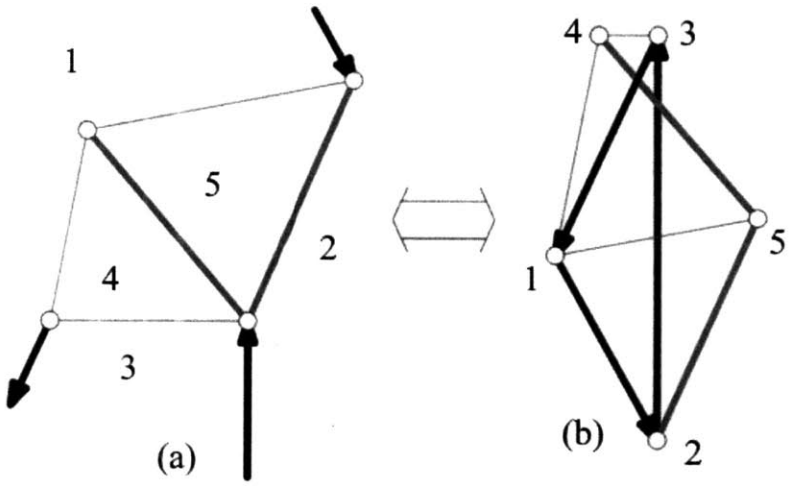

Figure 2-14. Graphic statics (a) form diagram and (b) force diagram (Fivet 2016)

The formation of these diagrams is dependent on the known parameters of the problem. For instance, it is possible to construct a form diagram from the force diagram or vice versa, but some initial values must first be determined. In most strut-and-tie models, the force diagram is constructed from a known form diagram, so this study will focus on that practice.

For any figure, the external forces must be in equilibrium. It is seen in Figure 2-14 (b) that the external forces in bold black lines form a closed force triangle, meaning the resultant force is zero (hence why it is termed "closed"). From there, any nodal point can be analyzed to check equilibrium. Starting with top force, an initial line of unknown length is drawn in the force diagram that is parallel to the incident force. In the

force diagram, this is the line from points 1-2. Each line on the force diagram relates to a line in the form diagram; whichever line is specified by the crossing of one space to another space in the form diagram (for instance, from space 1 to space 2, line 1-2 splits these spaces) corresponds to its force on the force diagram. So, for the top node of the form, lines 1-2, 2-5, and 5-1 form a closed force polygon. Since the force triangle is fully closed and the lines are parallel to those in the form diagram, the system is in static equilibrium.

Figure 2-15 shows a basic example for a triangular strut-and-tie model. In the form diagram on the left side, the angled members support a compressive force which they bring to the supports. A tension tie is needed to equalize the horizontal reaction at the supports. The force diagram begins with the external forces; the arrow representing F is drawn first at an arbitrary length. Then, the strut lines S_1 and S_2 are copied parallel from the form diagram onto the force diagram. The intersection of these lines S_1 and S_2 in the force diagram dictate the length of the lines and consequently the forces in those members. The tension force T_1 can also be found from this diagram as a horizontal line from the intersection of S_1 to the reaction forces R_1 and R_2 (not pictured below, each one half of F).

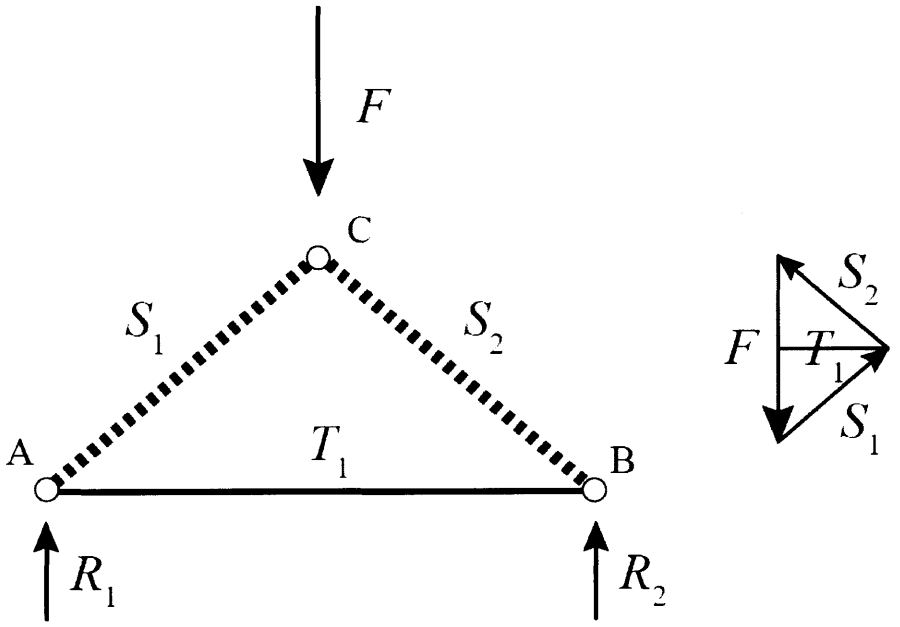

Figure 2-15. Graphic statics form and force diagrams to prove equilibrium (Kostic 2009)

Section 2.6 – Stress Fields in Wood Design

Using graphic statics in combination with strut-and-tie models yields accurate and discrete stress fields quickly and easily. However, when applied to wood design, there are several parameters that change

compared to concrete. As discussed previously, wood is an orthotropic material. Furthermore, contrary to reinforcement in concrete, it is difficult to directly reinforce timber in specific areas without complex equipment. As a result, strut-and-tie models through wooden beams take a slightly different appearance, but the principles and theorems behind stress field analysis and design still hold. These practices will be evaluated further in the Experiment Setup and Results sections of this study (Chapters 3 and 4, respectively).

While there has been limited work done in analyzing wooden structures with stress fields, there are a few studies which contribute to this field. In 2009, Dr. Martin Trautz proposed using self-tapping screws as reinforcement in wooden beams. Using the basis of stress field analysis, Trautz analyzes wooden beams with strut-and-tie models to identify the weakest areas of a beam and reinforces those locations with long self-tapping screws (2009). Although based on the theory of stress field analysis, Trautz employs finite element methods to dictate reinforcement location. Figure 2-16 depicts the finite element results of a tensile-loaded beam (a) in tension and (b) in compression as well as the strut-and-tie simplification with reinforcement layout in (c) and (d), respectively (Trautz 2009).

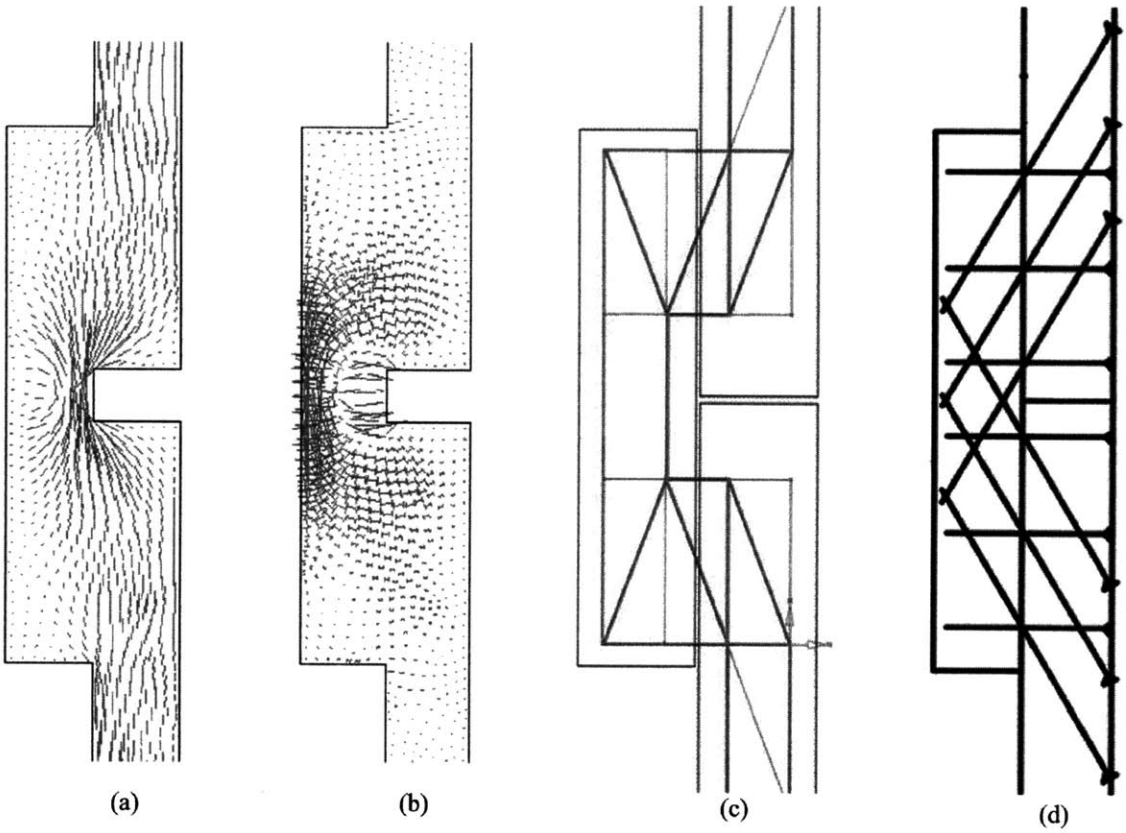

Figure 2-16. Finite element results for wooden beam loaded in tension showing (a) tension results and (b) compression results. Simplified strut-and-tie model shown in (c) with resulting reinforcement screws layout shown in (d) (Trautz 2009)

Setting up the actual dimensioning and construction detailing for this type of procedure, though, remains unfinished. The accuracy of this idealized approach also has yet to be evaluated. Despite its lack of final specification, however, this research proves promising; self-tapping screw reinforcement in a long-span timber beam showed an increase in bending capacity of roughly 80% (Trautz 2009). While additional research is necessary to supplement the findings in this study in order to carry it into actual practice, the initial findings are very useful.

Each of these concepts, then, can be synthesized into a process for characterizing wood specimens and connections using discontinuous stress fields. This work was largely explored analytically by Fivet (2012) and is investigated empirically in this thesis.

Chapter 3 – Experiment Setting

This chapter presents the exact reasoning behind testing decisions and provides a thorough overview of design criteria and result production. First, the theoretical design of the joint will be reviewed both symbolically and then with chosen dimensions. The construction sequence for the joint will also be investigated as well as the actual physical experimentation. In order to quantify the allowable strength used in all calculations, an investigation into the allowable design stress of the wood in question will be reviewed. Finally, the methodology behind strut-and-tie model construction will be revised and discontinuous stress field practices will be reviewed.

Section 3.1 – Literature Research of Joint

When considering the size and type of joint to analyze, a connection was desired that offered feasibility in current practice, ease of construction, and the ability to scale down to a testing application. As covered in previous chapters, there is extremely limited information in American design codes for wood-wood connection design, so additional research papers and industry-specific documentation were scoured for a suitable joint. The standard birdsmouth joint, pictured in Figure 3-1, was chosen for its constructability, scale-ability, and viability in modern timber framing design.

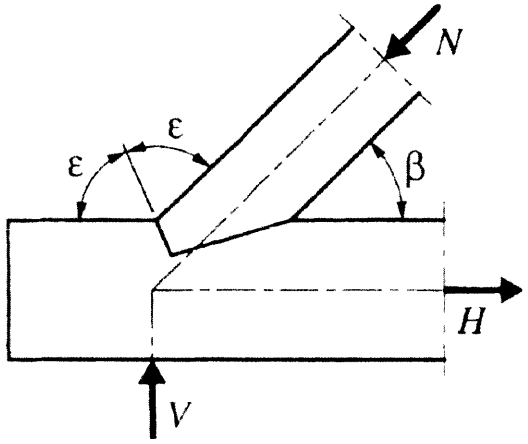

Figure 3-1. Birdsmouth joint diagram (Natterer 2000)

However, as the testing machines available at the Massachusetts Institute of Technology are predominantly axial compression machines, a slightly different design approach to the birdsmouth joint was needed. Because the machine available would be able to compress the joint axially, a new connection that resolved the resultant horizontal forces was desired. A diagram of the chosen joint is pictured in Figure 3-2.

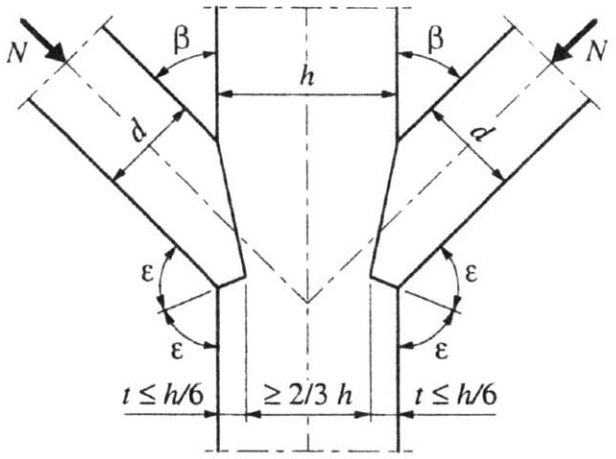

Figure 3-2. Double-birdsmouth connection diagram (Natterer 2000)

Although this connection detail is not presented in the American Wood Council codes, its strength and geometric guidelines are stated in a book by Julius Natterer in 2000. Geometrically, the joint is parameterized by a few key dimensions. As a double-birdsmouth connection is characterized by the same parameters as a standard birdsmouth detail, a single connection will be displayed and specified. As seen in Figure 3-3, a single birdsmouth connection is controlled by several parameters: *t, v, d, h, b,* and β.

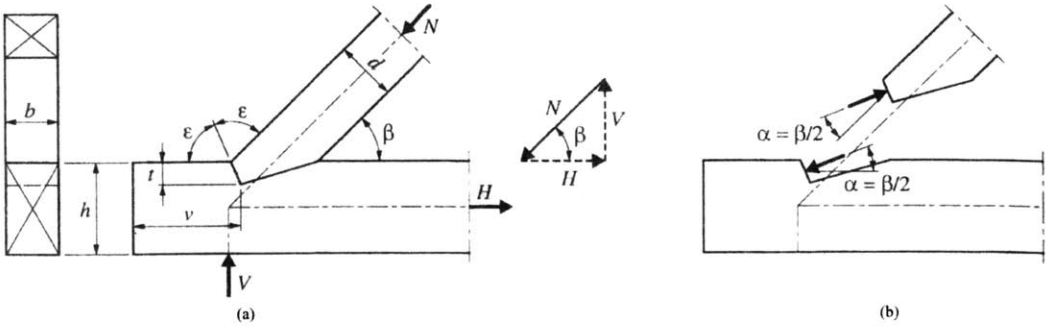

Figure 3-3. Key parameters in birdsmouth joint design (after Natterer 2000)

As indicated by the diagram, b is the depth of both the main beam and the arm of the joint. Furthermore, β is the angle between the arm and the beam. Although ε is listed as a parameter, it is simply given by Equation 3-1 as a function of β. Similarly, the angle α is given by Equation 3-2 and is the angle of the cut. The distance t is the purely vertical depth of cut into the beam while v is the horizontal distance from the end of the beam to the deepest cut location in the beam. Finally, the load N is the design load while V and H are the vertical and horizontal reaction resultants of N, respectively. While Natterer uses a design load to characterize the necessary dimensions of the beam, this study implements a predetermined geometry and then determines the allowable design load retroactively.

$$\varepsilon = 90 - \frac{\beta}{2} \; (Eq. 3-1)$$

$$\alpha = \frac{\beta}{2} \; (Eq. 3-2)$$

When looking at this specific joint, there are small differences between the theoretical behavior of the joint and its actual performance. As seen in Figure 3-4, there would in theory be a perfect division of the design load N into two forces, F_1 and F_2, which bear in compression onto their respective surfaces. When the joint rotates slightly, though, the force F_2 is completely eliminated, leaving all of the design force N to flow through the smaller bearing surface of the joint. The component of F_2, then, is translated mostly as bearing shear onto the small surface A (not indicated in Figure 3-4). The majority of the design force N still passes normal to the bearing surface A as F_3 shown in Figure 3-4 (b).

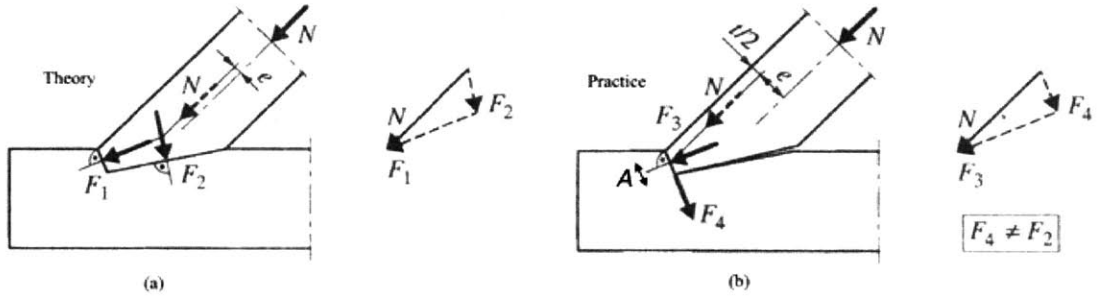

Figure 3-4. Flow of forces through standard birdsmouth connection in (a) theory and (b) practice (Natterer 2000)

The strength of the connection is controlled by three primary failure zones, and the lowest load that causes failure in one of these zones becomes the controlling region for the strength of the joint. Firstly, the bearing on the small surface A as seen in Figure 3-4 must be checked for allowable compressive load. Secondly, the end region of the beam must be checked for shear failure. Lastly, the width d of the arms of the connection must be checked as they can be significantly smaller and weaker than the central member. The failure modes can be seen in Figure 3-5.

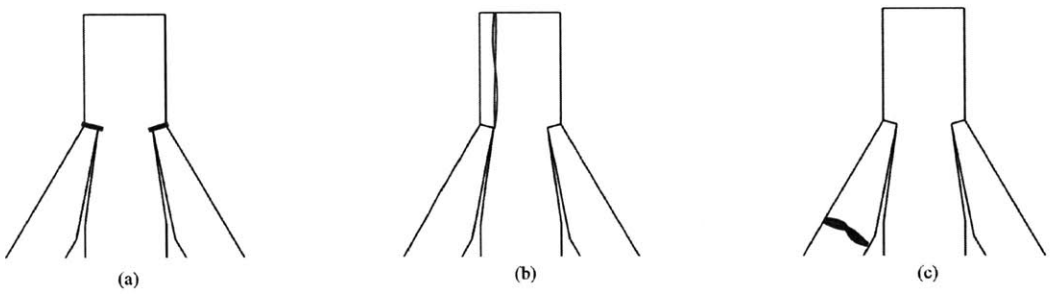

Figure 3-5. Failure modes for double birdsmouth connection in (a) crushing of tips, (b) shear of mast, and (c) crushing of arms

For the first failure mechanism, the area A can be calculated by Equation 3-3 where b is the depth of the wood, t is the depth of the connection, and β is the angle of the arms with respect to the central member.

$$A = \frac{b * t}{\cos\left(\frac{\beta}{2}\right)} \quad (Eq. 3-3)$$

The force F incident on the surface A as shown in Figure 3-6 is equivalent to the horizontal component of N divided by the bearing angle, $\beta/2$. The magnitude of this force is given by Equation 3-4. From the force F and area A, the stress on the inclined area A can be calculated. This stress is given by Equation 3-5.

$$F = \frac{H}{\cos\left(\frac{\beta}{2}\right)} = \frac{N_d \cos\beta}{\cos\left(\frac{\beta}{2}\right)} \quad (Eq. 3-4)$$

$$\sigma_{c,\alpha,d} = \frac{F}{A} = \frac{N_d \cos\beta}{b * t} \quad (Eq. 3-5)$$

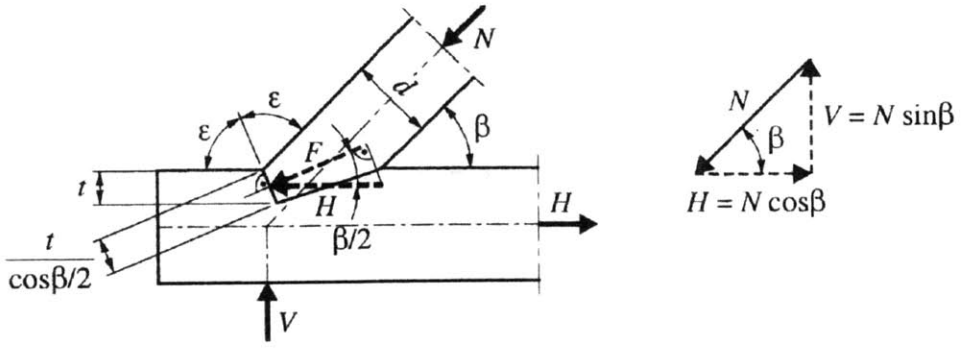

Figure 3-6. Detailed strength diagram of birdsmouth connection (Natterer 2000)

However, when given a geometry with material specifications and seeking the allowable design load N_d, Equation 3-5 can be arranged to solve for N_d as seen in Equation 3-6. As the value of t controls this failure mode, the failure load N is scripted as $N_{d,t}$ for clarity. It is also important to remember that wood is an orthotropic material, so the allowable compressive stress is dependent on grain angle; the α subscript on the stress $\sigma_{c,\alpha}$ denotes the material dependency on angle. Using the Hankinson formula explained in Chapter 2, the allowable stress $\sigma_{c,\alpha}$ can be calculated using Equation 3-7 depending on incident angle α. The values for $\sigma_{c,//}$ and $\sigma_{c,\perp}$ are the allowable compressive stresses parallel and perpendicular to the wood fibers, respectively.

$$N_{d,t} = \frac{\sigma_{c,\alpha} * b * t}{\cos\beta} \quad (Eq. 3-6)$$

$$\sigma_{c,\alpha} = \frac{\sigma_{c,\parallel} * \sigma_{c,\perp}}{\sigma_{c,\parallel} * \sin^2\alpha + \sigma_{c,\perp} * \cos^2\alpha} \quad (Eq. 3-7)$$

The second failure mode concerns shear in the end section of the beam. Although the dimension is not shown in Figure 3-6, the end beam length v can be recalled from Figure 3-3. Although v is specified to never drop below 6 in. (150mm), the otherwise minimum allowable shear length is given by Equation 3-8 (Natterer 2000). Similarly to the first failure mode, this equation can be transformed to calculate the allowable design load based on this failure criteria. This load is given the subscript $N_{d,v}$ to denote its dependence on shear failure, and its magnitude can be calculated by Equation 3-9. The allowable shear strength is denoted by τ_v.

$$v \geq \frac{N_{d,v} * \cos\beta}{b * \tau_v} \quad (Eq. 3-8)$$

$$N_{d,v} = \frac{\tau_{v,d} * b * v}{\cos\beta} \quad (Eq. 3-9)$$

Finally, the third failure mode is characterized by compressive crushing in the arms of the connection. Because the arms of a birdsmouth joint are almost always smaller than the main load-bearing beam, a strength check of the full side beam must be conducted. Equation 3-10 denotes the minimum value for d, the width of the side beams, and Equation 3-11 presents the transformation of this equation to come up with

the third design load, $N_{d,d}$. Similarly to the above example, $\sigma_{c,\beta}$ denotes the allowable compressive stress in the side members at an angle β to the grain, calculated using the Hankinson formula (Equation 3-7).

$$d \geq \frac{N_{d,d}}{b * \sigma_{c,\beta}} \ (Eq. 3-10)$$

$$d * b * \sigma_{c,\beta} = N_{d,d} \ (Eq. 3-11)$$

These three failure criterion control the strength characterization of this single-step birdsmouth joint. By solving for each design load $N_{d,t}$, $N_{d,v}$, and $N_{d,d}$, the minimum allowable load N for the system can be determined, fully distinguishing the overall strength of the joint. The controlling zones and their corresponding equations can be viewed in Table 3-1.

Table 3-1. Controlling failure zones for double birdsmouth joint

Failure Zone	Design Load	Load Equation
d	$N_{d,d}$	$d * b * \sigma_{c,\beta}$
v	$N_{d,v}$	$\frac{\tau_{v,d} * b * v}{\cos\beta}$
t	$N_{d,t}$	$\frac{\sigma_{c,\alpha} * b * t}{\cos\beta}$

Section 3.2 – Dimensioning of Experimental Joint

The three variables that have the least variability in design are h, d, and b. These dimensions are typically "chosen" first. In a two-dimensional projection, the value of b is unseen and is only used in allowable stress calculations. However, in a real three-dimensional world with full loading and utility, the beam depth b is obviously important. That being said, when testing and analyzing the strength of stress fields, a planar approximation is ideal, so a minimal depth was desired. As a result, a thickness of b of 0.75" was chosen (nominal 1" thickness by American lumber dimensioning). Standard sizes of d and h were also desired that were proportionally in line with practical use. Based on scaled precedents, values were chosen for 5.5" and 3.5" for d and h, respectively. Again, by American dimensioning practices, the nominal values for these boards are 6" and 4", respectively. Table 3-2 shows the dimensioning of b, d, and h in actual dimensions and nominal dimensions.

Table 3-2. Beam dimensions for designed connection

Dimension	Nominal Length (in.)	Actual Length (in.)
b	1.00	0.75
d	4.00	3.50
h	6.00	5.50
Connection Beam	1 x 6	0.75 x 5.5
Connection Arm	1 x 4	0.75 x 3.5

After finalizing the values for *b, d,* and *h,* the three remaining variables are *β, t,* and *v*. Holding each of the beam dimensions the same, these three "connection variables" dictate the shape and overall size of the connection. When considering the desired connection shape, the size and capabilities of the compressive load testing machine had to be evaluated. After a visit to the load testing laboratory, the testing bench was measured to have 30" by 30" square base, a 30" height, and an 8" diameter cylindrical top. From these restrictions, a joint was needed that fit into this 30" cube neatly and concisely. A Rhinoceros model was generated with the aid of Grasshopper that is fully parameterizable in order to explore a variety of geometries and dimensions that fit into the design space. While an infinite number of possibilities are viable as seen in Figure 3-7, a final geometry that fits closely within the geometric constraints and with regular dimensions was chosen. This joint geometry can be seen in Figure 3-8.

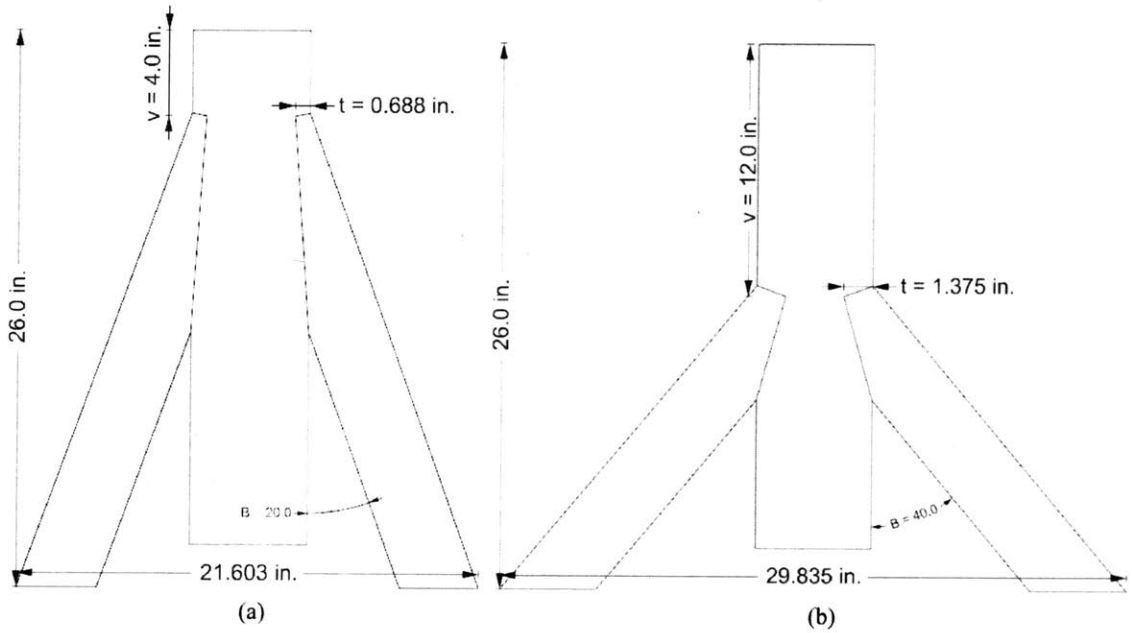

Figure 3-7. Examples of viable double-birdsmouth joints within geometric limitations with (a) 40° angle and (b) 20° angle

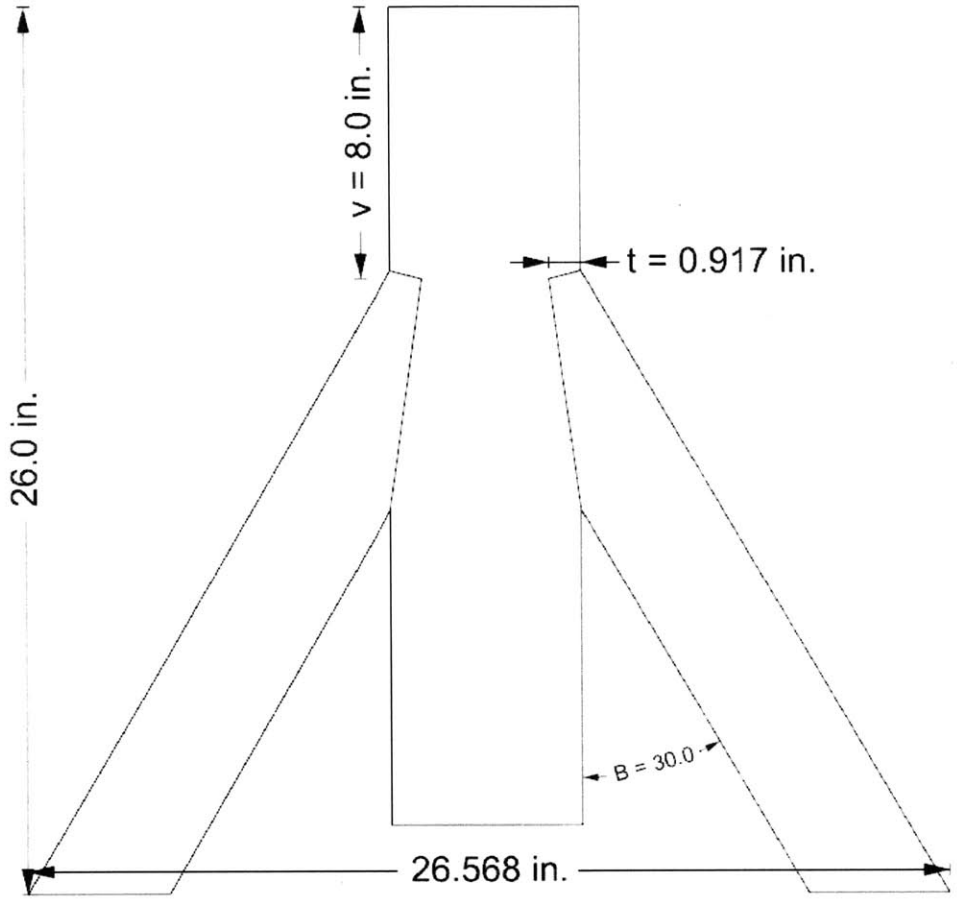

Figure 3-8. Final connection detail for double-birdsmouth connection

As seen in this chosen geometry, the angle β was set to an industry-common 30 degrees. In Natterer's study, the value of the joint depth t is limited to $h/6$ ($t \leq h/6$), so the value of t was derived from the previously chosen variable h (2000). A v was then chosen that maximized the size of the joint that fit within the restrained testing machine. Table 3-3 displays the variable values for the chosen connection.

Table 3-3. Chosen joint dimensions and corresponding coverage values

Dimension	Value (in)
v	8.0
t	0.917
β	30.0
Horizontal Coverage	26.6
Vertical Coverage	26.0

While the stress field provided by a straight compressive load on the top of the joint would be suitable for analysis, a more intricate stress field was desired that demonstrates the movement of stress throughout the entire central wooden beam. As such, a device was needed to transmit the compressive load from the top of the machine to another location within the central piece. This device, referred to as the transmission apparatus, was designed with doubly-thick wooden beams and a steel bar to fully transmit the loading down to a central point within the beam. A final schematic of the proposed design and the anticipated loading pattern is seen in Figure 3-9 and a diagram of the transmission apparatus can be found in Figure 3-10. A full physical view of the completed model can be seen with the transmission apparatus in Figure 3-11. The grain pattern displayed in all figures is solely an aesthetic rendering and has no significance to the actual grain orientation or pattern of the tested wood.

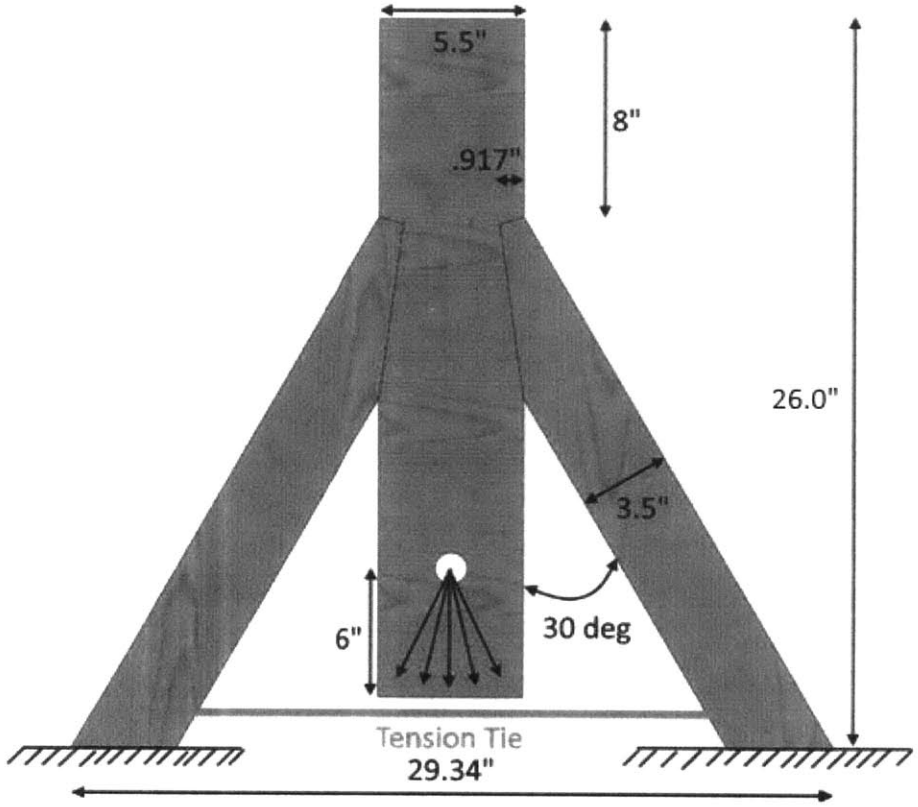

Figure 3-9. Full schematic of proposed birdsmouth connection

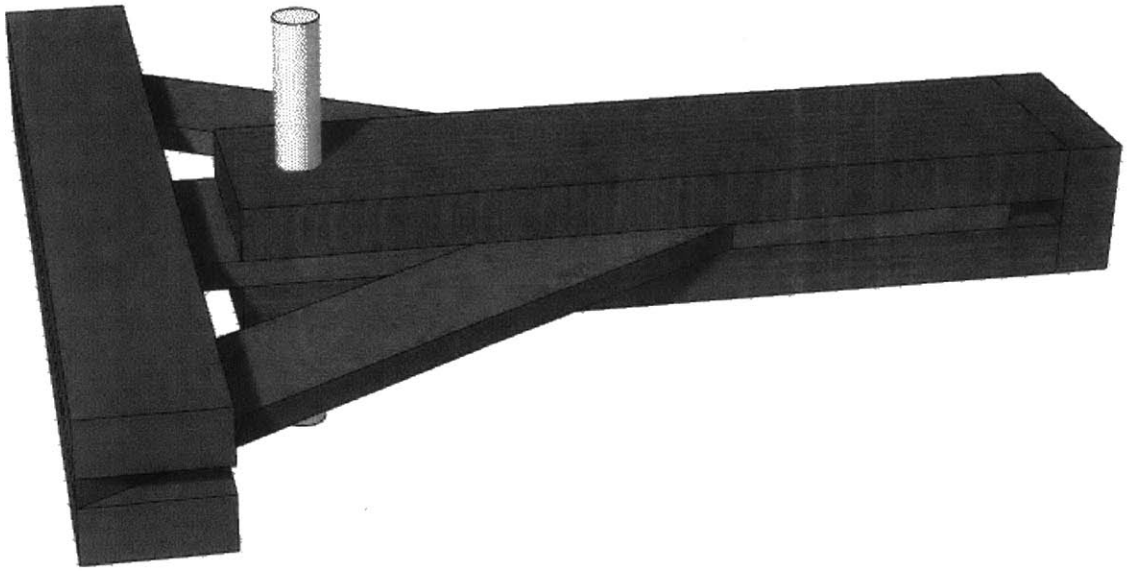

Figure 3-10. Transmission apparatus for buckling resistance with birdsmouth connection (digital view)

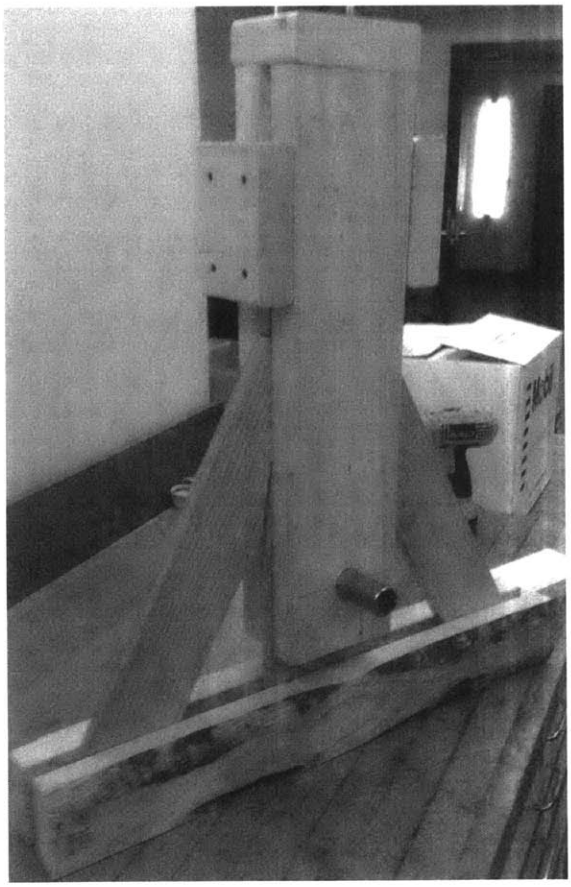

Figure 3-11. Transmission apparatus for buckling resistance with birdsmouth connection (actual view)

As seen in Figures 3-9 through 3-11, the transmission apparatus takes the compressive load induced by the machine and transmits it directly to a contact point on the central mast of the joint in testing. By relocating the positioning of this load, a more intricate and valuable stress field can be analyzed throughout the central member of the connection. The transmission apparatus also aids in holding the joint planar so that it does not buckle or deform out of shape. There are no connections between the transmission apparatus and the joint besides the steel bar passing through all members, so no additional fasteners inhibit or augment the strength of the connection in any way. Also, because of the horizontal reactions implicated by the connection, wooden tension ties are needed to help equalize the forces in the legs of the connection as seen in Figure 3-11.

In order to create perfect compression through the tip of the arms and eliminate any bearing between the long ends of the connection, a long section of the arms was cut out as seen in Figure 3-12. This modification to the original joint ensures that all the loading passes through the tip of the arm into the connection so that a more accurate stress field can be approximated with known loads and orientations.

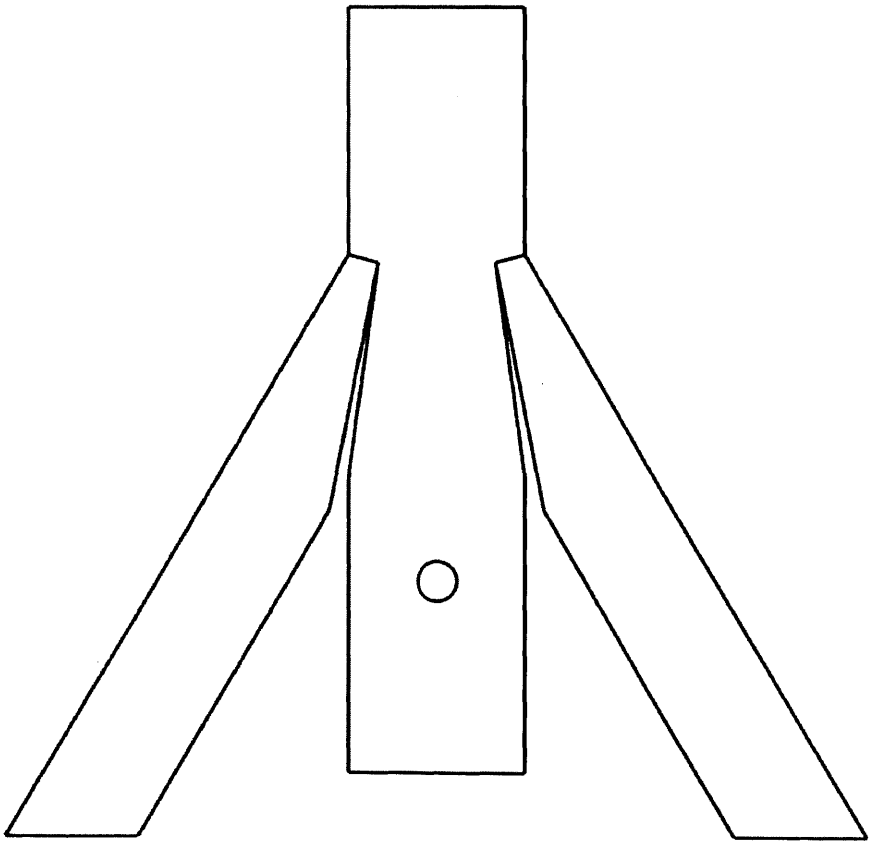

Figure 3-12. Modification of connection arms to ensure compression only through tip

After fully sizing a viable and testable joint, the geometric characterization according to Natterer's research could then be implemented to solve for a design load (Natterer 2000). As mentioned previously, while this research was aimed at designing joints for given loads and orientations, the process could be essentially reversed with a predetermined geometry to determine a controlling design load *N*.

Section 3.3 – Construction of Joint and Transmission Apparatus

In order to produce precise results between trials, wood samples were needed that were as pure of defects as possible. In order to decide on the best species and type of wood, a wood specialist named Ron Anthony of Anthony & Associates, Inc. was consulted (Anthony 2016). The recommendations by Mr. Anthony included using the clearest Douglas fir wood with as vertical of a grain pattern as possible. Although this caliber of wood is more expensive than standard graded lumber, its reliability and aversion to defects help keep its material properties as constant as possible throughout testing multiple specimens. As wood is very susceptible to local weakness due to deformities, clear, vertical-grain (CVG) Douglas fir was the best type of wood available. This CVG Douglas fir wood was obtained from Sterritt Lumber in Waltham, Massachusetts.

For repeatability of test results, three identical joints were constructed. The components of each connection included two identical side arms and one central mast. For three connections, then, six arms and three masts were needed. A template was cut to proper measurements out of hardboard and band sawed to the required specifications. Additionally, the 1.25" hole needed for the steel bar was cut using a hole-saw.

Using the hardboard templates, six connection arms and three masts were marked and cut using a table saw and band saw. The proper board dimensions of 1"x4" and 1"x6" boards were used for the arms and the masts, respectively. Because the transmission apparatus was more flexible in its dimensioning, standard 2"x6" and 2"x4" sections were used for the mast stabilizers and tension ties, respectively. These sections were cut using a standard table saw. A full picture of the transmission apparatus around a connection can be seen in Figure 3-13 (a).

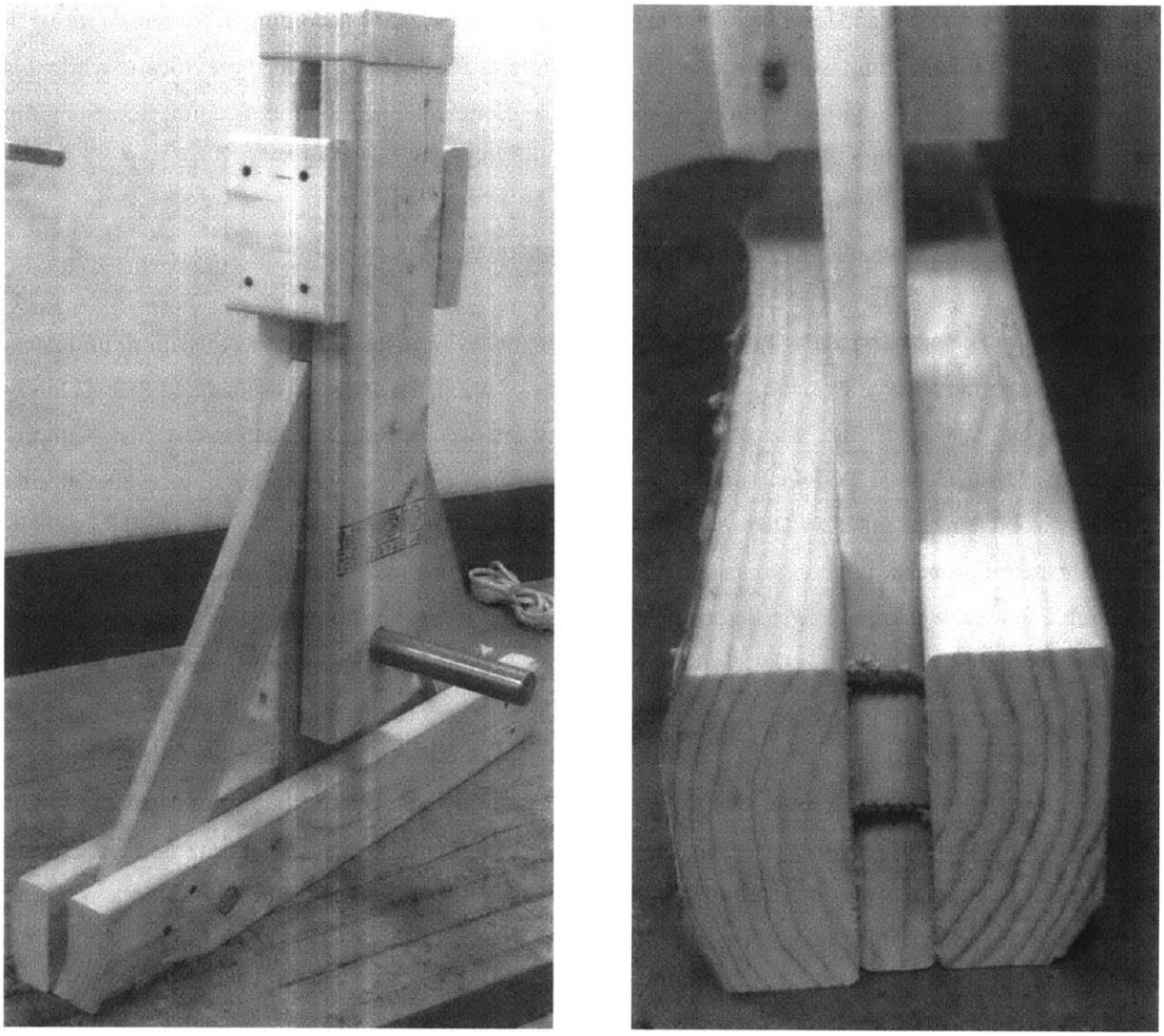

(a) (b)

Figure 3-13. Picture of (a) connection and transmission apparatus and (b) reinforcing screws at exterior

The transmission apparatus was fastened together using 2.5" steel screws as seen in Figure 3-13. Near the edges of the connection arms, additional screws were added as seen in Figure 3-13 (b) to help prevent the connection arms from bowing out and splitting. Because the stress field of only the central mast was analyzed, screws could be added to the connection arms that were far from the desired observation point.

Section 3.4 – Compressive Strength Tests of Joints

As mentioned previously, three identical joints were tested to ensure repeatability of data. The first joint was set up inside the transmission apparatus and the screws were added at the base of the connection arms to fix them at a set orientation. The steel rod was placed through the holes of both the central mast and the transmission apparatus to stabilize the system. The entire specimen was then placed on the load testing machine for testing as seen in Figure 3-14. This process was repeated twice more for a total of three joints.

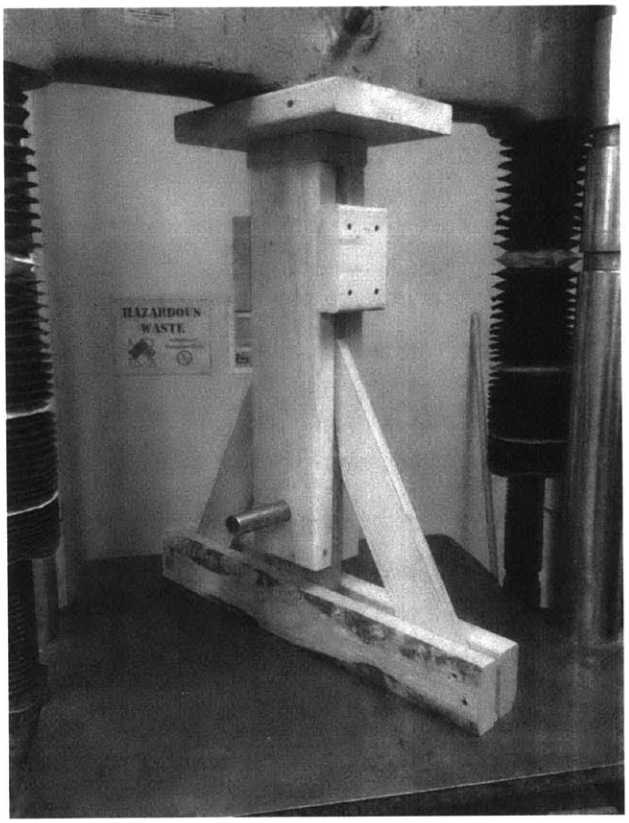

Figure 3-14. Connection prepared for compressive testing

Finally, as a test of the allowable compressive strength of the clear wood itself, three compressive tests were performed on 1"x1"x0.75" rectangular prisms parallel to the grain. The purpose of these tests was to serve as a benchmark to compare the compressive strength of the tested wood specimens to those found in documentation. A compressive loading setup for these small prisms can be seen in Figure 3-15.

Figure 3-15. Clear wood test for compressive strength parallel to the grain of the wood

Section 3.5 – Allowable Strength of Tested Specimens

While the American Wood Council and various other coding agencies provide values for the strength of wood species and sizes, these values are usually underestimates of wood strength for small-scale testing. As discussed in Chapter 2, materials, especially wood, tend to lower in effective strength as their dimensions go up due to the volume effect. As a result, large councils that are focused on construction and practice like the AWC use strength values that are often minimum-strength approximations which include safety factors for construction.

So, for the strength values of CVG Douglas fir, values were drawn from the ASTM materials testing documents, ASTM 2555.5152 (2015). These documents outline the strength values for clear wood specimens, making their application much more suited to small-scale analysis and design. As Sterritt Lumber is a provider of the Interior North sub-classification of Douglas fir timber, the initial design values for the CVG Douglas fir were extracted from Table 1 in the ASTM D2555.5152 specification. These charts provide all of the necessary values for stress field analysis including tensile and compressive strength

parallel and perpendicular to the grain as well as shear strength, and their values are presented numerically in Chapter 4.

However, because the values in these charts are for a very wide range of samples and regions, the compressive tests mentioned in the previous section served to further quantify the specific strength of the actual timber used for testing. As outlined in Chapter 4 of this thesis, the values of the compressive tests were used to scale all other allowable strength values for the clear wooden specimens used. This modification aimed for a much more accurate and particular strength approximation than just the ASTM D2555.5152 could provide.

Section 3.6 – Stress Field Approximations

As discussed in previous sections, stress fields were used to analyze the forces flowing through the central mast and to determine a maximum design force N that could be compared to physical and code-prescribed limits. Discrete stress field approximations were made in an iterative manner to continually increase the allowable load throughout the system. A sample strut and tie model along with its force diagram can be seen in Figure 3-16.

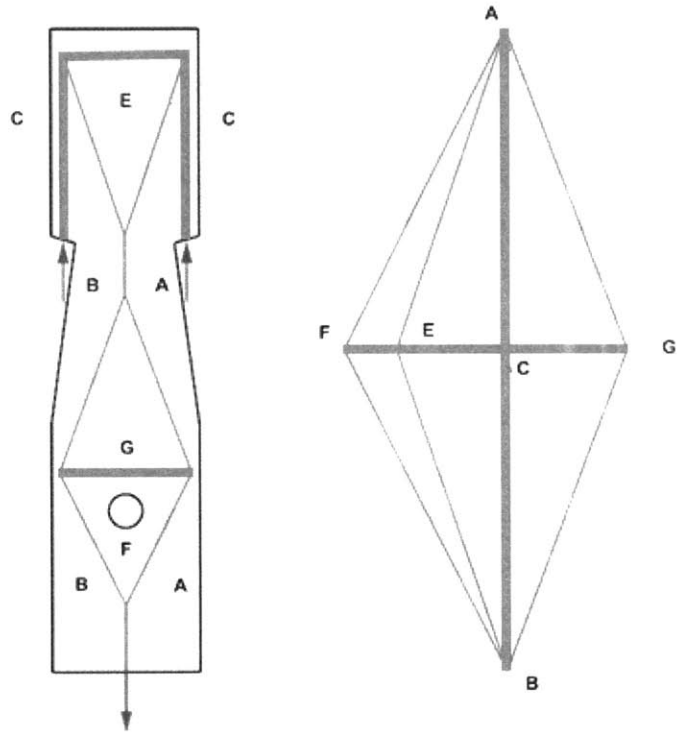

Figure 3-16. Sample strut and tie model with force diagram through central mast

Using intuition, an initial stress field was "guessed" for the flow of forces through the central mast, and topological and geometrical variations are produced subsequently. The forces were drawn as lines with thin denoting tension and thick compression. External forces were drawn with arrowheads for clarification. The force diagram with corresponding colors can be seen on the right side of Figure 3-16. As covered in Chapter 2, the length of the lines in the force diagram correspond to the magnitude of the forces in those members; as such, it is easy to compare the relative forces through various sections of the mast.

While the compressive force is transmitted to the lower hole in the mast, a simple approximation to move that force to the lower section of the mast was made to simplify calculation. Due to the limitations of graphic statics, a force vector crossing through the diagram (as it would be applying a compressive force at the hole) creates additional considerations and constraints within the force diagram, so this simplification was made to ease computation.

From this model, then, several things can be extrapolated to obtain the failure load. Referring back to plastic design in Chapter 2, if a discontinuous stress field can be constructed in which all stress fields remain within the bounds of the geometry, then this field is a lower bound to the failure load. As such, stress fields can be iteratively drawn to increase the load throughout the mast until the highest allowable load is found. In the initial model seen in Figure 3-16, there are several parameters that control this load. The methodology of determining these parameters and their implications are covered below.

Each strut or tie in the form diagram should be assigned a notation. In this analysis, the designation of each line is determined by the two labelled fields surrounding it; for instance, the lowest tension tie on the form diagram as seen in Figure 3-16 is termed *A-B* as it is the line dividing sections *A* and *B*. Similarly, the lower compression strut is titled *F-G* as it divides sections *F* and *G*. Consequently, the force diagram denotes the force of line *F-G* as the distance between the two points *F* and *G*. Labelled areas on the form diagram correspond to specific points on the force diagram.

After each strut or tie has been assigned a title, its angle relative to the grain of the wood should be determined as well as its status in tension or compression. Since wood is indeed orthotropic, the allowable stress within the section changes based on angle as well as direction of loading, so designating the loading orientation and angle to the grain becomes essential. The allowable stress for each section depending on grain angle and direction of loading can then be established by the use of the Hankinson formula and the allowable stresses within the wood itself.

The magnitude of the force within the member is also important and is measured by the length of the line on the force diagram. The length of the applied force can be normalized to one, and all other forces scaled off of this value. An artificial "stress field ratio" is created and given by Equation 3-12. In this ratio, $\sigma_{allowable,i}$ is the allowable stress within the strut or tie dependent on angle and loading direction, P_i is the force in that member, and $\sigma_{normalized}$ is the normalized stress field according to the initial force. This ratio is important in the determination of the controlling stress field width.

$$R_{\sigma,i} = \frac{\frac{P_i}{\sigma_{allowable,i}}}{\sigma_{normalized}} \quad (Eq. 3-12)$$

As discussed in Chapter 2, the width of the stress field is dependent on the allowable geometric constraints in the form diagram. The section width which first violates this geometric constraint is termed the controlling section, and all other stress field widths are scaled off of this segment. In concrete design, the controlling region is simply the one with the shortest length to the boundary of the surface. However, in wood design, the allowable stress changes per orientation and direction of load, so the controlling section is not as intuitively identified. For instance, a section with a larger allowable stress field width that is perpendicular to the grain could still be a controlling region compared to a much smaller allowable stress field width parallel to the grain.

Because this controlling region is difficult to intuitively observe, it must be quantified for direct comparison. From the form diagram, the smallest allowable width to a boundary surface can be easily measured for each strut or tie. An example of this measurement can be seen in Figure 3-17. As seen in the diagram, the controlling width for tie *A-F* is equal to 0.33. Although the bottom width of *A-F* could extend to 3.07, the full stress rectangle must fit within the constraints of the geometry, so 0.33 becomes the limiting width.

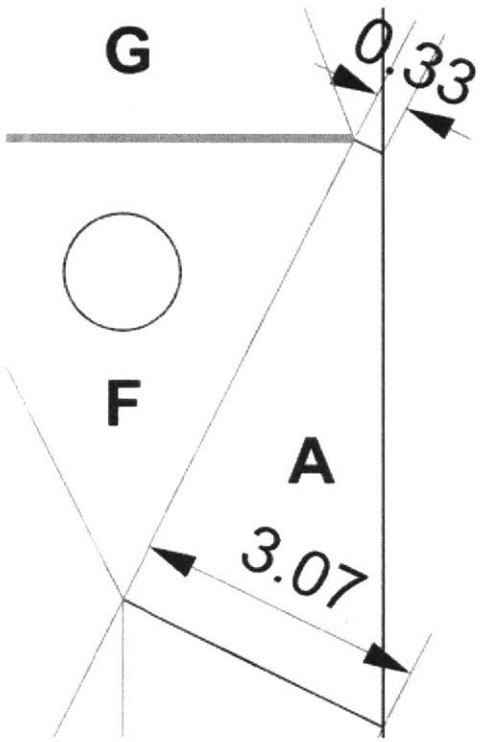

Figure 3-17. Example dimensions of allowable stress field widths

All of these maximum stress field widths can then be tabulated and used in conjunction with the stress field ratio given by Equation 3-12 to determine the controlling stress field width. Using these two values, the field width ratio can then be determined by Equation 3-13 for each individual strut and tie. In this equation, $R_{\sigma,i}$ is the stress field ratio, $w_{\sigma,max,i}$ is the maximum allowable stress field width determined by the geometry, and $R_{L,i}$ is the field width ratio.

$$R_{L,i} = \frac{w_{\sigma,max,i}}{R_{\sigma,i}} \quad (Eq. 3-13)$$

The strut or tie with the lowest field width ratio is the controlling stress field within the model and all other stress field widths should be scaled from this dimension. Equation 3-14 should be used in order to find the stress field width of every strut and tie. $R_{\sigma,i}$ is the stress field ratio of the strut or tie in question, $R_{\sigma,controlling}$ is the controlling stress field ratio, and $w_{i,\alpha,max}$ is the maximum stress field width of the strut or tie in question. w_i, then, is the resulting stress field width based on the controlling field.

$$w_i = w_{i,\alpha,max} \frac{R_{\sigma,i}}{R_{\sigma,controlling}} \quad (Eq. 3-14)$$

With the stress fields fully dimensioned and sized, the loading throughout each strut or tie at the limit state of the specified stress field can be easily calculated by Equation 3-15. Furthermore, the external load F on the system can be quantified in a similar manner. This external load is the quantified failure load of the system under the given strut-and-tie model.

$$F = w_i * \sigma_{allowable,i} \ (Eq. 3-15)$$

As discussed previously, from here, it is an iterative process to continually design strut-and-tie models to give higher failure loads until the physically-observed failure mode is reached. The iterative analyses of sequential stress fields can be found in Chapter 4 of this thesis.

While these strut and tie models effortlessly account for the tension and compression inside the wood, the shear forces are much more difficult to portray. Using Mohr's circle and stress transformation equations, though, it is possible to calculate the shear inside each strut or tie (Fivet 2012). As seen in Figure 3-18, Mohr's circle can be solved both graphically and symbolically for the shear stress. The shear transformation equation can be found in by Equation 3-16.

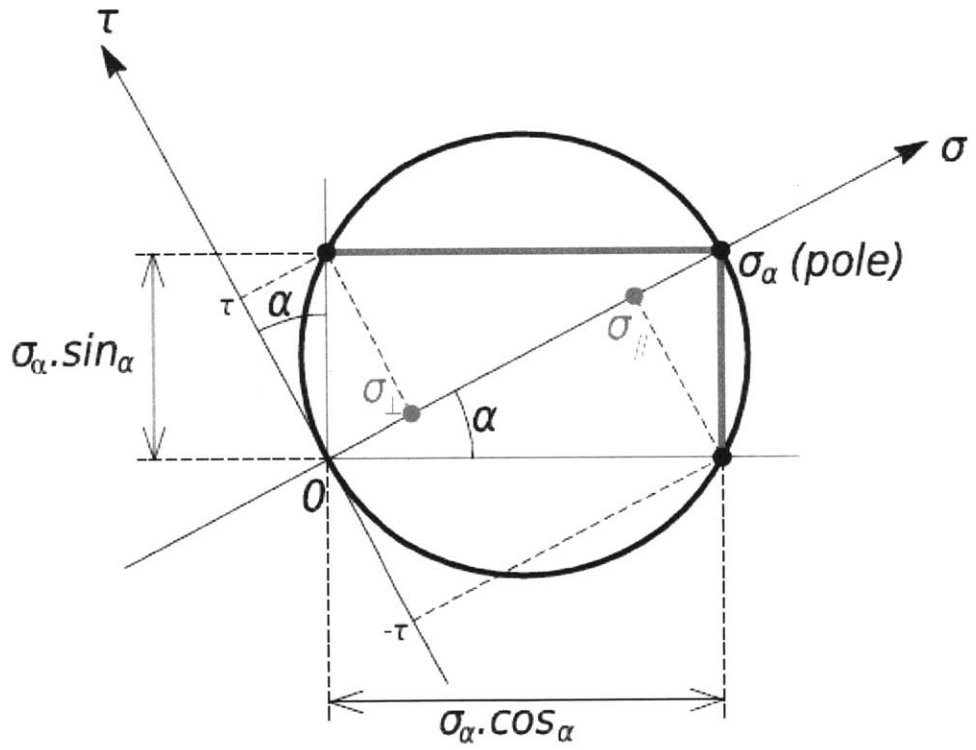

Figure 3-18. Mohr's circle for wood specimen at an angle α to the grain (Fivet 2012)

$$\tau_\alpha = \sigma_\alpha * \sin\alpha * \cos\alpha \ (Eq. 3-16)$$

From Equation 3-16, it is very easy to calculate the shear stress within each strut and tie. The allowable shear stress also follows the Hankinson formula. These two shear values, the actual shear within the member and the allowable shear at that angle α, can be compared to determine if shear failure will occur within each strut or tie.

Chapter 4 – Results

This chapter offers the results from the physical tests, code approximations, and stress field approximations in a sequential order. The outcomes of these three approaches are analyzed in more depth in Chapter 5, however quick observations between the results are made in this section.

Section 4.1 – Physical Tests

The three physical tests yielded remarkably similar results. As covered in Chapter 3, there were three governing failure criteria: crushing of the small contact area, crushing of the central mast, and shear of the end section of the mast. With each test being set up identically with the same constraints, failure by shear was observed in all three connections. In the first test, however, the shear was not observed in the top of the mast as expected; it was instead seen where the steel bar contacts the central mast. While in a different location, this failure mode is actually very similar to the shear of the top mast as they have similar tear-out distances. Pictures of the fractured connections can be seen in Figure 4-1 (a), (b), and (c) for tests 1, 2, and 3 respectively.

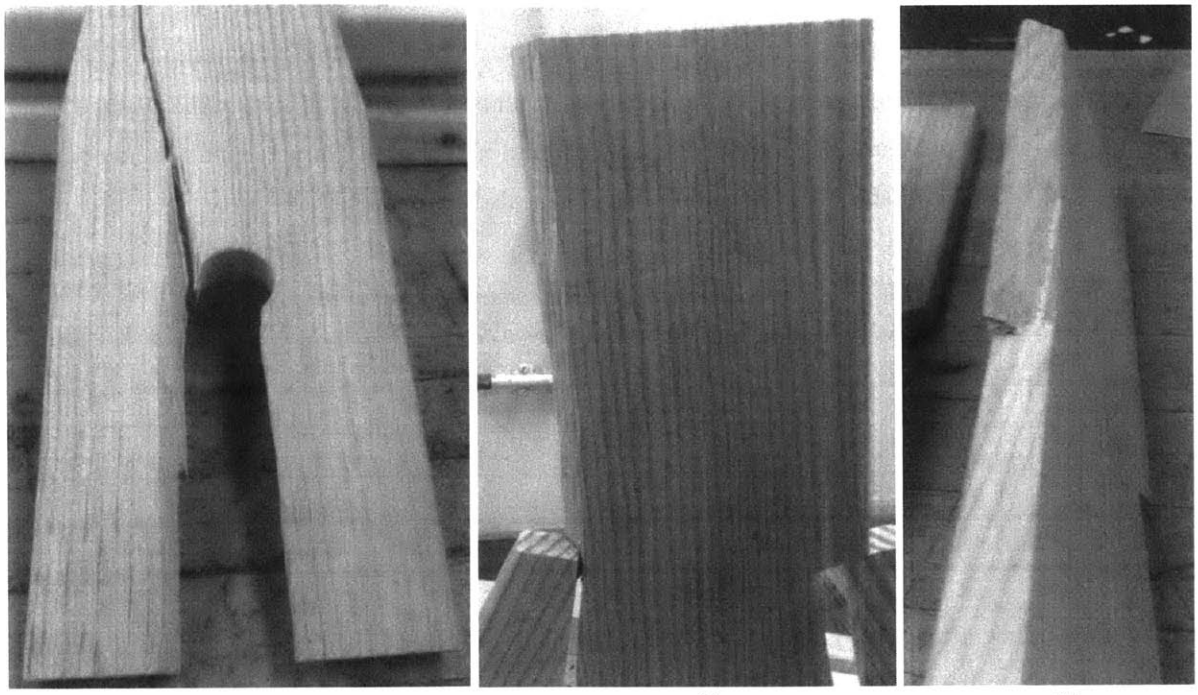

(a) (b) (c)

Figure 4-1. Failure modes for experimental connections (a) Test 1, (b) Test 2, and (c) Test 3

As seen by Figure 4-1, each of the connections suffered from shear failure. This failure mode is characterized by sudden, brittle failure at the limit state with little deformation or indication of failure prior to fracture. The load-deflection diagram for the three tests can be found in Figure 4-2.

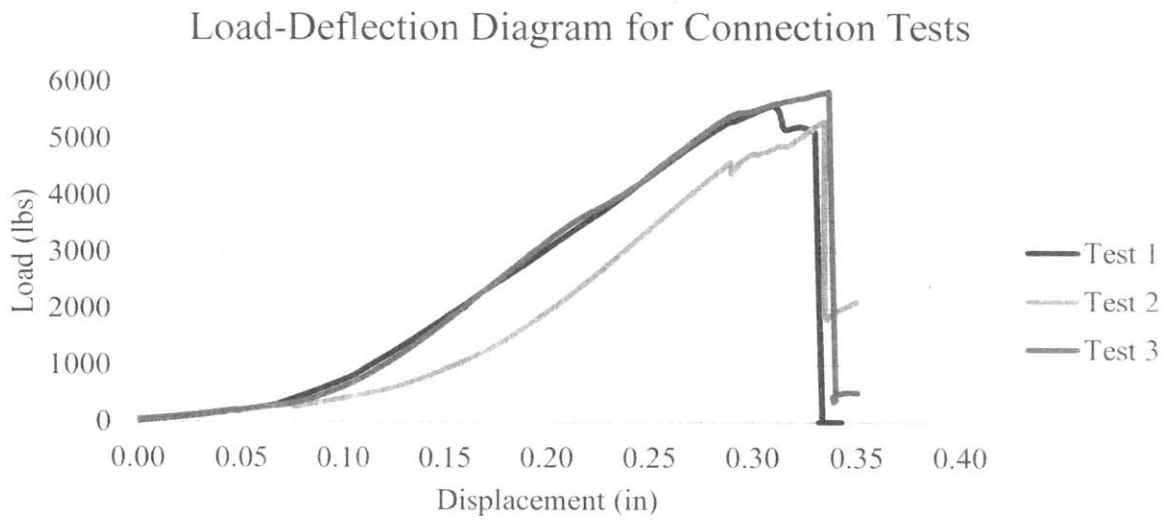

Figure 4-2. Load-deflection diagram for birdsmouth joint tests

Referring to Figure 4-2, the tests results are very precise. All three tests fall within 5% of the average failure strength of the joint. The failure load for each test can be found in Table 4-1. The percent difference between the failure load of each test and the average failure load can also be found below.

Table 4-1. Failure strength of tested connections and average

Test Number	Failure Load *F* (lb)	Displacement (in)	Percent Difference from Average (%)
Test 1	5583	0.310	0.19
Test 2	5307	0.335	4.89
Test 3	5828	0.336	4.48
Average	5573	0.327	3.19

Additionally, as mentioned in Chapter 3, compressive tests were performed on three small rectangular sections taken from the test pieces of wood in order to determine the allowable compressive strength of these segments. The load-deflection diagram for each of the blocks can be seen in Figure 4-3 and the corresponding data can be seen in Table 4-2. As seen in the diagram, the strength values for these tests are

a bit less precise than the data gathered for the connections testing, but their values are still within suitable deviation.

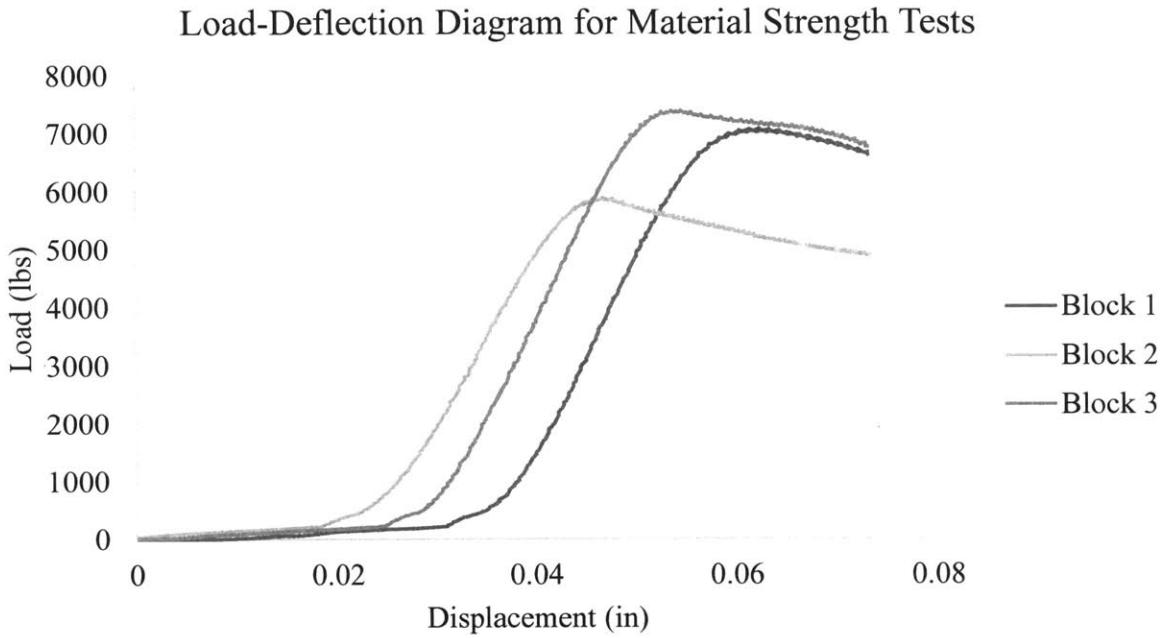

Figure 4-3. Load-deflection diagram for material strength tests

Table 4-2. Compressive failure strength of 1"x1"x0.75" clear specimens parallel to the grain

Test Number	Max Strength (psi)	Displacement (in)	Percent Difference from Average (%)
Test 1	9436	0.063	4.14
Test 2	7863	0.047	14.08
Test 3	9863	0.054	8.55
Average	9053	0.055	8.921

According to these tests, then, the allowable compressive strength parallel to the grain for a 1"x0.75" specimen is equal to 9050 psi. While these three tests seem relatively consistent with each other, this crushing strength is vastly different than that given by ASTM 2555.5152, which is 3469 psi. In fact, the experimental crushing strength is roughly 250% of the ASTM given value. While partly this strength discrepancy is explained by the superior quality of the clear, vertical grain wood used, the large disparity between strength values and the absence of tests to obtain the actual tension and shear stress values makes comparison between code-prescribed strength and experimental strength difficult.

As a result, the clear wood values from ASTM 2555.5152 were used for all calculations and approximations for code considerations as well as stress field procedures. While the compressive strength given in Table 4-2 may provide a slightly closer approximation to the actual design strength of the CVG Douglas fir, its sporadic results and inconsistency with ASTM standard make it less reliable. In order to provide an identical comparison between characterization methods, a uniform set of wood properties given by ASTM 2555.5152 was used. The values used are shown in Table 4-3.

Table 4-3. Allowable strength values for CVG Douglas fir according to ASTM 2555.5152

Loading Type	Allowable Strength (psi)
Compression ∥	3469
Compression ⊥	669
Tension ∥	7438
Tension ⊥	313
Shear ∥	947
Shear ⊥	325

In summary, the physical tests of this birdsmouth joint yielded three shear failures all very close to 5.5 kips. Shear governed the failure of this connection for every trial in a very consistent manner. Furthermore, while compressive tests were performed to analyze the allowable strength of the tested wood, the original ASTM values were chosen because of their consistency and reliability.

Section 4.2 – Code Approximations

As discussed in Chapter 3, the double birdsmouth joint is characterized by three critical zones and can fail in three different ways. The connection can fail by the crushing of the contact area, noted $N_{d,t}$; the shearing of the end section, noted $N_{d,v}$; or the crushing of the side arms, noted $N_{d,d}$. The equations governing these failure criteria are detailed in Chapter 3 but are reproduced below in Table 4-4.

Table 4-4. Controlling failure zones for double birdsmouth joint

Failure Zone	Design Load	Load Equation
d	$N_{d,d}$	$d * b * \sigma_{c,\beta}$
v	$N_{d,v}$	$\frac{\tau_{v,d} * b * v}{\cos\beta}$
t	$N_{d,t}$	$\frac{\sigma_{c,\alpha} * b * t}{\cos\beta}$

The allowable design load $N_{d,d}$ is given by the geometry of the arm and its allowable compressive stress. Because nominal 1"x4" boards were used in this experiment, the actual dimensions for d and b correspond to 3.5" and 1.5", respectively. The allowable compressive stress is found using the Hankinson formula with an angle β of 30° and the design values for allowable stress dictated by the ASTM. Ultimately, with the given geometry and stress values, this design load $N_{d,d}$ comes out to 4450 lb and corresponds to the maximum compressive stress in the arms of the connection.

Similarly, the allowable load $N_{d,v}$ is given by the shear length at the end of the mast, v. With a v of 8" as given in the predetermined geometry, the design equation for $N_{d,v}$ can be solved for a connection strength of 6560 lb. This value corresponds to the maximum shear stress in the free end of the mast.

Finally, the last parameter can be calculated from the connection depth t. Using the design equation for $N_{d,t}$, a maximal compressive load on the bearing area A is found to be 2150 lb. This design strength dictates the allowable load before crushing occurs in the tips of the connection at the small bearing surface. The three allowable design loads are tabulated in Table 4-5 for the given geometry and material properties.

Table 4-5. Allowable loads for critical areas of connection

Failure Zone	Design Load	Load Equation	Allowable Load (lb)
d	$N_{d,d}$	$d * b * \sigma_{c,\beta}$	4450
v	$N_{d,v}$	$\frac{\tau_{v,d} * b * v}{\cos\beta}$	6560
t	$N_{d,t}$	$\frac{\sigma_{c,\alpha} * b * t}{\cos\beta}$	2150

The minimum design load out of these three failure scenarios then becomes the controlling and expected mode of failure. However, the failure load N does not correspond exactly to the external load on the system; in other words, N is not equivalent to the load observed from testing, F. In order to draw a comparison between these two forces, the direction of N must be dictated clearly. The orientation of the external force F as well as the design load N can be seen in Figure 4-4. As the angle between these members is β, the relationship between F and N can be given simply by Equation 4-1.

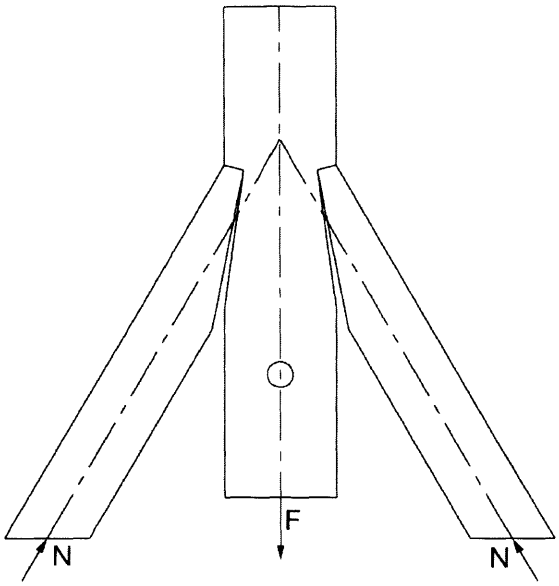

Figure 4-4. Design force N compared to external force F

$$F = 2 * N \cos\beta \quad (Eq. 4-1)$$

Using Equation 4-1, the design loads N_d can then be converted to allowable external loads F. In other words, the failure mechanisms expected from the design loads N are now viewed in terms of the imposed machine load F. The ultimate external loads for each failure mode can be seen in Table 4-6.

Table 4-6. Allowable external loads for critical areas of connection

Failure Zone	External Design Load	Predicted Failure Load (lb)
d	$F_{d,d}$	7710
v	$F_{d,v}$	11360
t	$F_{d,t}$	3720

These values will be compared with those of the experimental results in Chapter 5.

Section 4.3 – Stress Field Approximations

Overall, stress field analyses yielded similar results to that of the code (Natterer 2000). Several stress fields (a) through (f) that iterate towards the maximum discovered failure load in (g) can be seen in Figure 4-5. In Table 4-7 the maximum design load for each of these fields can be found according to the methods set in Chapter 3.

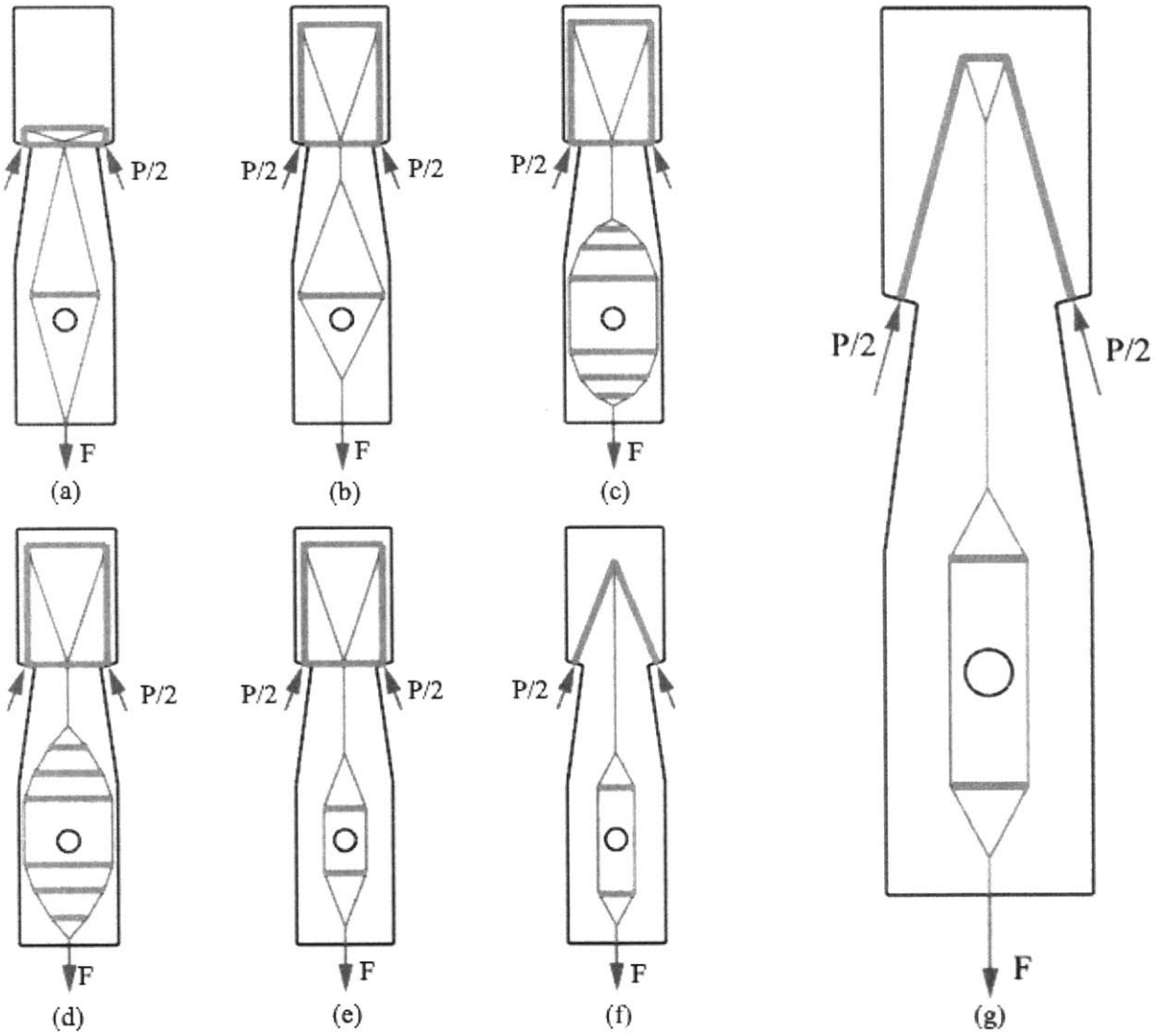

Figure 4-5. Strut-and-tie models of allowable stress field distributions through central mast

Table 4-7. Allowable load F for stress fields (refer to Figure 4-5 and 4-6)

Stress Field	Maximum Allowable Load *F* (lb)
(a)	273
(b)	1301
(c)	689
(d)	956
(e)	3383
(f)	3162
(g)	3729

In trials (a) through (e), the external forces *P/2* were resolved through the use of a vertical and horizontal compression strut in the top of the mast. However, this approximation is invalid due to the nature of the problem; as such, the force *P/2* is estimated to pass perpendicularly through the bearing surface *A* as seen in fields (f) and (g). Because of this limitation, the top compression struts in model (g) are the controlling regions of stress where the strut contacts the edge of the model.

As mentioned in Chapter 3, though, the shear forces throughout the mast are not as visible from a strut-and-tie model. The shear must be checked at each strut and tie to ensure that failure does not occur due to shear before tensile or compressive failure. The equations for the shear within each member and the allowable shear within that member can be found in Chapter 3. For each of the models shown in this section, shear was checked to be within the allowable limits. The analysis of shear failure can be found in Chapter 5.

However, one interesting discovery about the nature of shear stress in strut-and-tie models is that it is characteristically difficult to quantify. When drawing a strut-and-tie model, shear is neglected. However, in an orthotropic material such as wood, shear could sometimes cause failure before tensile or compressive failure. Because shear strength is also dependent on the Hankinson formula, the shear in a member can be expressed as a function of its allowed stress as indicated in Chapter 3 as well as a function of its orientation and loading direction. Because a strut or tie is loaded to its maximum allowable stress, these values are independent of the actual force magnitude inside the member. If the maximum allowable shear at every angle is then plotted according to the Hankinson formula and compared against the shear caused by the maximum allowable compressive and tensile stresses, a range can be determined in which the shear stress will control failure in the strut and tie model. This plot can be seen in Figure 4-6.

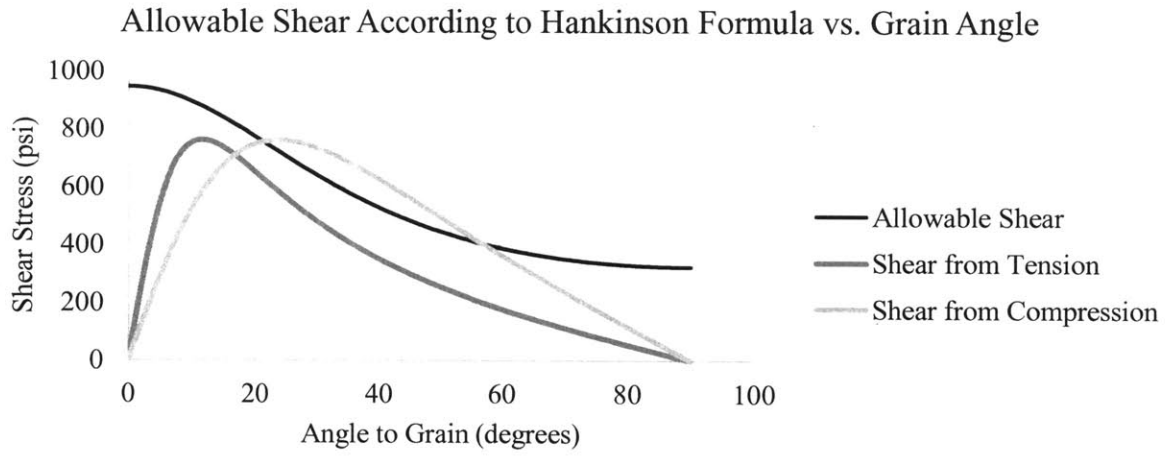

Figure 4-6. Allowable shear from Hankinson formula compared to shear caused from allowable tensile and compressive stresses

As seen in Figure 4-6, the shear caused from the maximum allowable tensile stress nowhere violates the allowable shear from the Hankinson formula. In other words, a given tie would always fail from tension before it would fail from shear according to this model. However, when considering compressive struts, there is a range from about 22° to 56° in which shear failure would occur before compressive failure. As a designer this doesn't necessarily mean that compressive struts at these angles are off-limits but rather that they need to be designed for shear failure instead of compressive failure. In other words, the thickness of the stress strut must be widened according to the shear strength instead of the compressive strength.

Additional testing on specimens are required to validate this model as it is heavily dependent on the type of wood being used. In practice such a shear strength also depends on the capacity of the wood outside the stress fields that contain it. While this 22° to 56° range is suitable for Interior North Douglas fir, other species have different ratios between their tensile, compressive, and shear strengths, so these values should be checked before assumptions are extrapolated. For the most part though, the most critical zone is in compression at a roughly 30° angle to the grain. Here, the allowable compressive stress is still quite large while the allowable shear starts to drop off. For tension, on the other hand, the allowable tensile stress is so low that as the angle increases, the allowable tensile strength plummets, making the resulting shear rather low. This serves as an explanation as to why the shear stress from tension never rises above the cutoff limit.

Overall, this chapter demonstrates that for the given material properties in this connection, shear failure dominated the physical testing. Conversely, both the code and stress field assumptions predicted crushing failure in the tips before shear failure in the central mast. These results are investigated further in Chapter 5.

Chapter 5 – Discussion

This chapter serves as an analysis of the observed results. In this chapter, the strength approximations from both prior research and the stress field analyses will be compared to the physical testing performed and to each other.

Section 5.1 – Comparison of Design Approaches

Assuming the same geometric constraints and material properties, the failure loads for each method of testing can be seen in Table 5-1. The physical failure load is listed as the average between all three tests while the others are the strengths found from their respective applications.

Table 5-1. Failure load and mode for each test method

Test Method	Physical Testing	Code Approximation	Stress Field Analysis
Failure Load (F) (lb)	5573	3725	3729
Anticipated Failure Mode	Shear of Mast	Crushing of Tip	Crushing of Tip

As seen in the testing results, the physical loading limit is significantly higher than either the code approximation or the stress field analysis. Furthermore, the mode of failure observed in testing was not the controlling failure mode predicted by the code or the stress field analysis. While these differences are certainly unexpected, they can be attributed in part to a few extraneous considerations.

Possibly the largest dilemma is in the actual mode of failure. According to the research done by Natterer (2000), while the crushing of the tip is anticipated at 3725 lb for this geometry, the shear failure of the end section of the mast shouldn't occur until 11360 lb. The shear failure observed in the physical tests is roughly half of this value at 5573 lb. So, although the code does expect failure prior to the empirical load recorded, the joint not only failed in the shear region where it supposedly had more strength but also *didn't* fail where it was predicted to in crushing.

This discrepancy could partly be explained by the fact that all structural connections are several orders of magnitude larger than the tested connection. Code approximations typically apply to much larger material tests and account for lower quality wood including safety factors and other considerations already factored in, so a lower anticipated strength than the observed failure mode should be expected. However, this justification is meager at best as the expected shear failure is almost exactly twice the observed amount.

Because of this extreme difference in shear strength, the code-prescribed requirements for this joint design are insufficient and should not be used for a connection of this magnitude.

With stress fields, on the other hand, the predicted shear failure is much more consistent with the physical tests. Although stress fields similarly showed that crushing should first be seen in the contact area between the arms and the mast before shear failure, the magnitude of the shear failure occurs shortly afterwards. Because there was no observed crushing in the arms or the mast, the compressive strength of the wood is obviously an underestimate of its actual strength. So, it is an easy conclusion that the compressive strength does not control in this case. If this compressive strength is raised, then, the stress field model presented in Chapter 4 predicts a shear failure at a compressive load F of 4619 lb. The expected failure loads for crushing and shear for each method of analysis can be found in Table 5-2.

Table 5-2. Observed and anticipated failure loads for different analysis approaches to birdsmouth connection

Test Method	Physical Testing	Code Approximation	Stress Field Analysis
Crushing Failure Load (F_t) (lbs)	--	3725	3729
Shear Failure Load (F_v) (lbs)	5573	11360	4619

As seen in Table 5-2, while neither prediction was verified by the crushing at roughly 3700 lb in the physical test, the observed shear in the empirical testing is much closer to the 4620 lb estimate provided by the stress fields. Furthermore, when considering wood strength values and their scalability, the results from the stress field analysis make even more sense. Since no crushing was observed in the connection, the compressive strength of the wood used in this analysis is obviously higher than the value provided by the ASTM 2555.5152 standard. While this increase usually also corresponds in an increase in all other wood strength properties as well, the compressive strength increases at a much faster rate than the shear strength. In other words, if the compressive strength of a sample increases by 30%, the shear strength may only be augmented by 10%.

From this explanation, it is easy to draw that if the compressive strength no longer controls the failure mode of the connection because of its augmented strength, then shear will be the next failure mode. With a slightly increased shear strength, then, the 4619 lb approximation may raise to something in the 5500 lb range, making stress fields a very accurate and viable analysis method. However, the specific material properties need to be fully characterized and known in order to make accurate stress field guesses. Otherwise, it is difficult to get clear, straightforward approximations that correspond with empirical testing.

In general, though, almost all theory in wood analysis is an approximation with key assumptions. The Hankinson formula is the result of a smattering of tests and, while accurate, is a purely empirical formula for wood design. However, since wood grows as a living material, no two pieces of wood are identical, meaning the properties of two wood specimens even from the same species can be very diverse. When trying to characterize the strength of wood, then, large margins of difference are observed between species and grades of lumber. Stress field analysis assumes perfectly anisotropic material and a unified, homogeneous grain oriented perfectly vertically, so small deviations in the grain orientation could affect the approximations provided by the stress fields. Because of these limitations, although an upper-bound approach would help to assess the stress field analysis with regard to the physical theory, it is extremely difficult to predict exact upper-bound failure of wooden joints. Conversely, though, the lower-bound approach as detailed above seems to have provided an accurate picture and provided safe joint designability compared to the code.

Section 5.2 – Guidelines for Stress Field Design and Future Work

As mentioned in the previous section, it becomes incredibly important to know the material properties of the tested wood as precisely as possible. The stress field approach, while accurate, depends heavily on these properties being accurate. Furthermore, when considering a strut-and-tie model through a wooden connection, a comparison should be made similar to Figure 4-6 which presents the allowable strut angles which don't need shear analysis. As covered previously, any strut inside the critical range presented in Figure 4-6 is actually controlled by shear failure instead of compressive failure. Having the exact material properties to make this comparison, then, becomes even more important.

Again, though, these strut angles aren't strictly off-limits for design, they just simply must be designed for shear failure instead of compressive failure. For each species or grade analyzed with the stress field approach, a chart similar to Figure 4-6 should be reproduced for both tension and compression and the critical ranges recorded.

After these guidelines for shear are set forth, the analysis of the joint is comparatively simple and is an exercise similar to that of concrete design. When iterating the discontinuous stress field model until a controlling region is found, using the largest amount of space within the given geometry usually corresponds to a "better" stress field approximation. Additionally, these stress field models may be used to design any type of connection as they can be specified independently of geometry. Knowing the material properties of the wood in question again becomes paramount in the designability of these joints.

Chapter 6 – Conclusions

The main objective of this thesis was to decipher if discontinuous stress field analyses could be used to accurately model the forces flowing through a wooden member and joint. To answer this question, the strength approximations from a stress field analysis were compared to both empirical testing as well as prior research estimates provided in the code.

Three joints were tested and each failed from shear stresses in the central mast. This result was initially surprising as both stress field models and the prescribed code predicted failure in compression at the tips of the connection. However, the connection never physically failed in crushing, only in shear.

While the code indeed predicted failure below the observed joint strength, this failure happened in shear, an unexpected mode where the joint was anticipated to have almost double additional shear strength, and *not* in crushing as projected. A stress field analysis, on the other hand, provided a much clearer picture of the theoretical joint strength as it compares to the physical testing. Although a stress field analysis similarly predicted crushing first at an almost identical load as the code, the next failure mode of shear corresponded much more closely to the observed value.

The lower-bound results found from the stress field analysis can be investigated further with knowledge of wood material properties to give an even closer estimate to the allowable strength design of joints. Because no crushing was observed in the connection, the compressive strength of the wood is therefore higher than the ASTM-dictated standards. This consequently raises the shear strength by a small amount. While the exact material properties of the wood are unknown, a large rise in compressive strength and a small increase in shear strength are both reasonable approximations for the type of wood used and directly correlate to the test loads observed. With a much higher compressive strength, crushing would not have occurred in the bearing surface as predicted. Moreover, with a higher shear strength, the predicted 4620 lb shear failure could raise even closer to the observed average 5570 lb failure.

From these results, it is reasonable to dictate that discontinuous stress field approximations may be used as a suitable design method for wood to wood joints. When designing these joints, knowing the exact material properties becomes possibly the most important aspect of design and safety factors must be set with great care. Furthermore, the designer needs to ensure that shear stress does not dictate failure. While it is hard to see shear in a strut-and-tie model, a simple diagram can be constructed limiting the angles for compressive struts to a certain range where shear controls. With these guidelines, designing for shear becomes nothing

more than staying within allowable limits or, if passing into the shear-controlled region, designing for shear failure. Again, knowing the exact material properties helps to make this range as precise as possible.

References

Allen, Edward, Wacław Zalewski, and Nicole Michel. *Form and Forces: Designing Efficient, Expressive Structures*. Hoboken, NJ: John Wiley & Sons, 2010. PDF.

Anthony, Ron. "Wood Science Discussion." Telephone interview. 17 Mar. 2016.

Breakey. "Metrics and the Basics of Mechanics." *Sustainability Workshop*. N.p., 12 Mar. 2008. Web. 25 Apr. 2016.

Brunner, Maurice. "On The Plastic Design of Timber Beams with a Complex Cross-Section." (2000): p. 1-5. WTCE, Canada. Swiss School of Engineering for the Wood Industry. Web. 25 Sept. 2015.

Drucker, D. C. "On Structural Concrete and the Theorems of Limit Analysis (Technical Report) Unknown Binding – 1960." *On Structural Concrete and the Theorems of Limit Analysis (Technical Report): Amazon.co.uk: Daniel C Drucker: Books*. N.p., n.d. Web. 24 Apr. 2016.

Eng. Toolbox. "Softwood Lumber - Dimensions." Engineering Toolbox, n.d. Web. 25 Apr. 2016.

Eng. Toolbox. "Engineering Materials." Engineering Toolbox, n.d. Web. 25 Apr. 2016.

Fivet, Corentin. "Recherche des modalités permettant l'étude des assemblages en bois par manipulation graphique de champs de contraintes discontinus." (2012): p. 1-97. Université catholique de Louvain. PDF.

Fivet, Corentin. "Graphic Statics: Introduction." (presentation, MIT 1.S979 Interactive Structural Form-Finding, Cambridge, MA, March 7th, 2016).

Gvozdev 1938; 1960

Hankinson, R. L. *Investigation of Crushing Strength of Spruce at Varying Angles of Grain*. Washington: U.S. GPO, 1921.

Heyman, Jacques. *Basic Structural Theory*. Cambridge: Cambridge UP, 2008.

Kollmann, Franz Friedrich Paul, and Wilfred A. Côte. "Chapter 1: The Structure of Wood and the Wood Cell Wall." *Principles of Wood Science and Technology*. Berlin: Springer-Verlag, 1968. N. pag. PDF.

Marti, Peter. "Basic Tools of Reinforced Concrete Beam Design." *ACI Journal Proceedings JP* 82.1 (1985): n. pag. PDF.

Muttoni, A., J. Schwartz, and Bruno Thürlimann. *Design of Concrete Structures with Stress Fields*. Basel: Birkhäuser, 1997. PDF.

Natterer, Julius, Jean-Luc Sandoz, Martial Rey, and Maurice Fiaux. *Construction En Bois: Matériau, Technologie Et Dimensionnement*. Lausanne: Presses Polytechniques Et Universitaires Romandes, 2000. PDF.

Risen, Clay. "The World's Most Advanced Building Material Is... Wood." *Technology*. Popular Science, 6 Feb. 2014. Web. 11 Apr. 2016.

Ritter, Michael A. "Chapter 3: Properties of Wood and Structural Wood Products." *Timber Bridges: Design, Construction, Inspection, and Maintenance*. Washington, DC: U.S. Dept. of Agriculture, Forest Service, Engineering Staff, 1990. N. pag. MN DOT. PDF.

Ruiz, Miguel F., and Aurelio Muttoni. "On Development of Suitable Stress Fields for Structural Concrete." *SJ ACI Structural Journal* 104.4 (2007): n. pag. PDF.

Schlaich, Jorg, Kurt Schafer, and Mattias Jennewein. "Toward a Consistent Design of Structural Concrete." *PCI Journal* 32.3 (1987): 74-150. PDF.

Weibull, W., Fatigue Testing and Analysis of Results, Pergamon Press, 1961.

Standard Practice for Establishing Clear Wood Strength Values. West Conshohocken, PA: ASTM International, 2015. PDF.

National Design Specification for Wood Construction. Washington, D.C.: Association, 2015. PDF.

"U.S. EIA - Independent Statistics and Analysis." *How Much Energy Is Consumed in Residential and Commercial Buildings in the United States?* U.S. Energy Information Statistics, 6 Apr. 2016. Web. 11 Apr. 2016